REPORT NO. 8

SEMI-ANNUAL PROGRESS REPORT

1 January 1966 to 30 June 1966

STUDIES IN FUNDAMENTAL CHEMISTRY OF FUEL CELL REACTIONS

NsG-325

Submitted to:

NATIONAL AERONAUTICS AND SPACE ADMINISTRATION

Washington 25, D. C.

Submitted by:

Professor John O'M. Bockris

The Electrochemistry Laboratory
The University of Pennsylvania
Philadelphia, Pa. 19104

NOTICE

This report was prepared as an account of Government sponsored work. Neither the United States, nor the National Aeronautics and Space Administration (NASA), nor any person acting on behalf of NASA:

A.) Makes any warranty or representation, expressed or implied, with respect to the accuracy, completeness, or usefulness of the information contained in this report, or that the use of any information, apparatus, method, or process disclosed in this report may not infringe privately owned rights; or

B.) Assumes any liabilities with respect to the use of or for damages resulting from the use of any information, apparatus, method or process disclosed in this report.

As used above, "person acting on behalf of NASA" includes any employee or contractor of NASA, or employee of such contractor, to the extent that such employee or contractor of NASA, or employee of such contractor prepares, disseminates, or provides access to, any information pursuant to his employment or contract with NASA, or his employment with such contractor.

TABLE OF CONTENTS

PROJECT PERSONNEL

Section I

Mr. Boris Cahan, Pre-Doctoral Research Fellow

Dr. Halina Wroblowa, Supervisor

Section II

Miss Rowshan Jahan, Pre Doctoral Research Fellow

Dr. Aleksandar Damjanovic, Supervisor

Section III

Mr. Shyam Argade, Pre Doctoral Research Fellow

Dr. Eliezer Gileadi, Supervisor

Section IV

Dr. Ljerka Duic, Post Doctoral Research Fellow

Dr. Halina Wroblowa, Supervisor

Section V

Dr. S. Srinivasan, Post Doctoral Research Fellow

Dr. John O'M. Bockris, Supervisor

ABSTRACTS

SECTION I. THE MECHANISM OF VARIOUS TYPES OF HIGH RATE ELECTRODES

Previously found localization of current within a narrow region of meniscus was utilized to construct electrodes containing very small amounts of catalyst placed in the critical regions.

In hydrogen oxidation the rate was limited only by the ohmic resistance of the electrode matrix; in oxygen reductions, the rate was activation controlled up to 100 mA cm^{-2}.

SECTION II. THE MECHANISM OF ELECTROCATALYSIS

Noble metal electrode (Pt, Rh, Pd, Ir and Au) surfaces were carefully examined to confirm previous results in Fe^{+++}/Fe^{++} reaction. Further, it was established that Fe^{+++}/Fe^{++} reaction occurs on oxide free electrodes of the above metals. Also the heats of adsorption on these metals were calculated for this reaction.

SECTION III. POTENTIAL OF ZERO CHARGE

In order to meet the criticism of Frumkin et. al. [3] on the measurements on potentials of zero charge on platinum reported from this laboratory,[1,2] critical tests were carried out to establish the correctness of the previous results.

SECTION IV. ADSORPTION IN THE DOUBLE LAYER WITH SPECIAL REFERENCE TO THERMAL EFFECTS

Potential sweep method and single galvanostatic pulse method were used to determine adsorption of ethylene and benzene from aqueous solutions at various temperatures. Results of the two electrochemical methods are compared and their equivalency is experimentally shown. A method of correcting potential-sweep results for the change in oxide coverage in presence and absence of organic adsorbate is proposed.

Results of electrochemical methods of measuring adsorption are compared with those obtained by radiotracer measurements.

SECTION V. ELECTRODE KINETIC ASPECTS OF ELECTROCHEMICAL ENERGY CONVERSION

During this period a paper entitled "The Theory of Porous Gas Diffusion Electrodes" was written and a Chapter entitled "Electrochemical Techniques in Fuel Cell Research," to appear in the Hand Book of Fuel Cell Technology, was completed.

SECTION I. THE MECHANISM OF VARIOUS TYPES OF HIGH RATE ELECTRODES

As indicated in Report No. 7, (NsG-325), the computer solution of the differential equations for the "finite contact angle meniscus" yields a linear relationship between applied voltage and current output, in excellent agreement with experimental observations. One is tempted to apply the label "ohmic" to any system with a linear E-I relationship. It must be stressed that in this case "pseudo-ohmic" is a more accurate term. The computer data has been analyzed to give the graphs of Fig. 1 and Fig. 2, for hydrogen and oxygen respectively.

The half-current point distance (the distance from the edge of the meniscus within which 50% of the total current is produced)is plotted against applied potential, η_{app}, and against the potential at the tip η_t. (Note: this distance is really an area, $A_{1/2}$, since all computations are done per linear cm of meniscus.) Within this region, complete diffusion depletion does not occur, and the current is primarily activation limited.

Figures 1 and 2 show an important result of the computer calculation. At moderate to high polarizations, the reaction zone is extremely small (10^{-3} to 10^{-6} cm long), far smaller than the area predicted by the "thin film" theory. Since it is difficult to make porous electrodes much thinner than 10^{-2} cm and/or to control the deposition of catalyst in this region, much of the catalyst is thus outside of the useful region.

An optimally utilized catalyst, therefore, would be in a very thin region of the electrode and would exhibit Tafel behavior, since almost no diffusion limit could occur.

Electrodes prepared in this fashion by deposition of thin films on a supporting porous matrix have been produced, and exhibit this expected behavior.

With catalyst loadings of only 10 $\mu g/cm^2$ of Pt, Tafel behavior of oxygen reduction has been followed up to currents of 100 mA/cm^2. Residual true ohmic resistance due solely to the electrolyte matrix obscured the behavior at higher currents.

In case of hydrogen ionization, where i_o is several orders of magnitude higher, the current was limited only by the ohmic resistance of the matrix. Experiments are in progress with thinner matrices.

Up to now, with the same loading (10 $\mu g/cm^2$ of Pt) currents up to 400 mA/cm^2 have been obtained.

Legends for Figures

Fig 1 Dependence of half-current area on applied potential and on tip potential as calculated for Hydrogen.

Fig 2 Dependence of half-current area on applied potential and on tip potential as calculated for Oxygen.

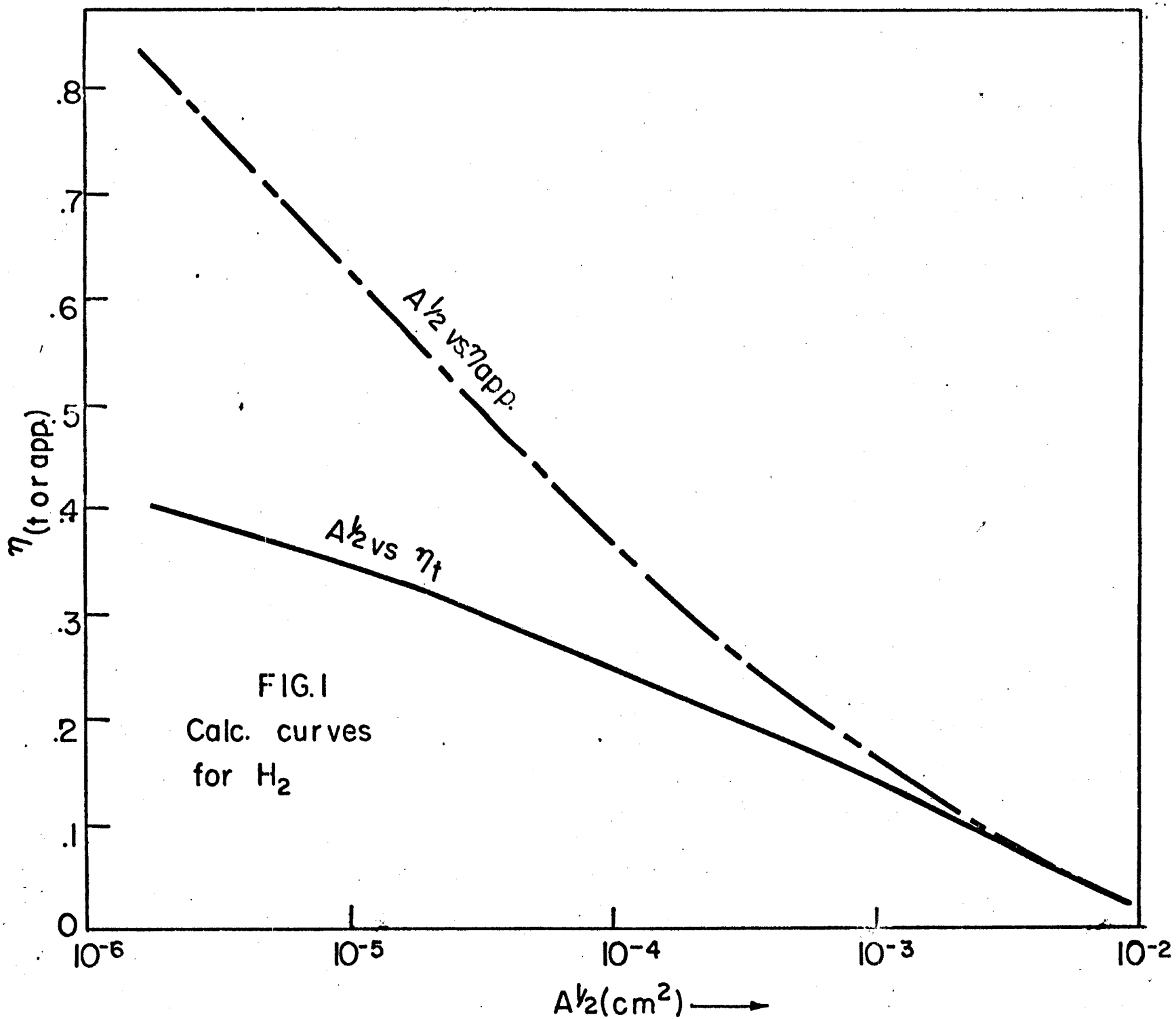

FIG. 1
Calc. curves
for H_2

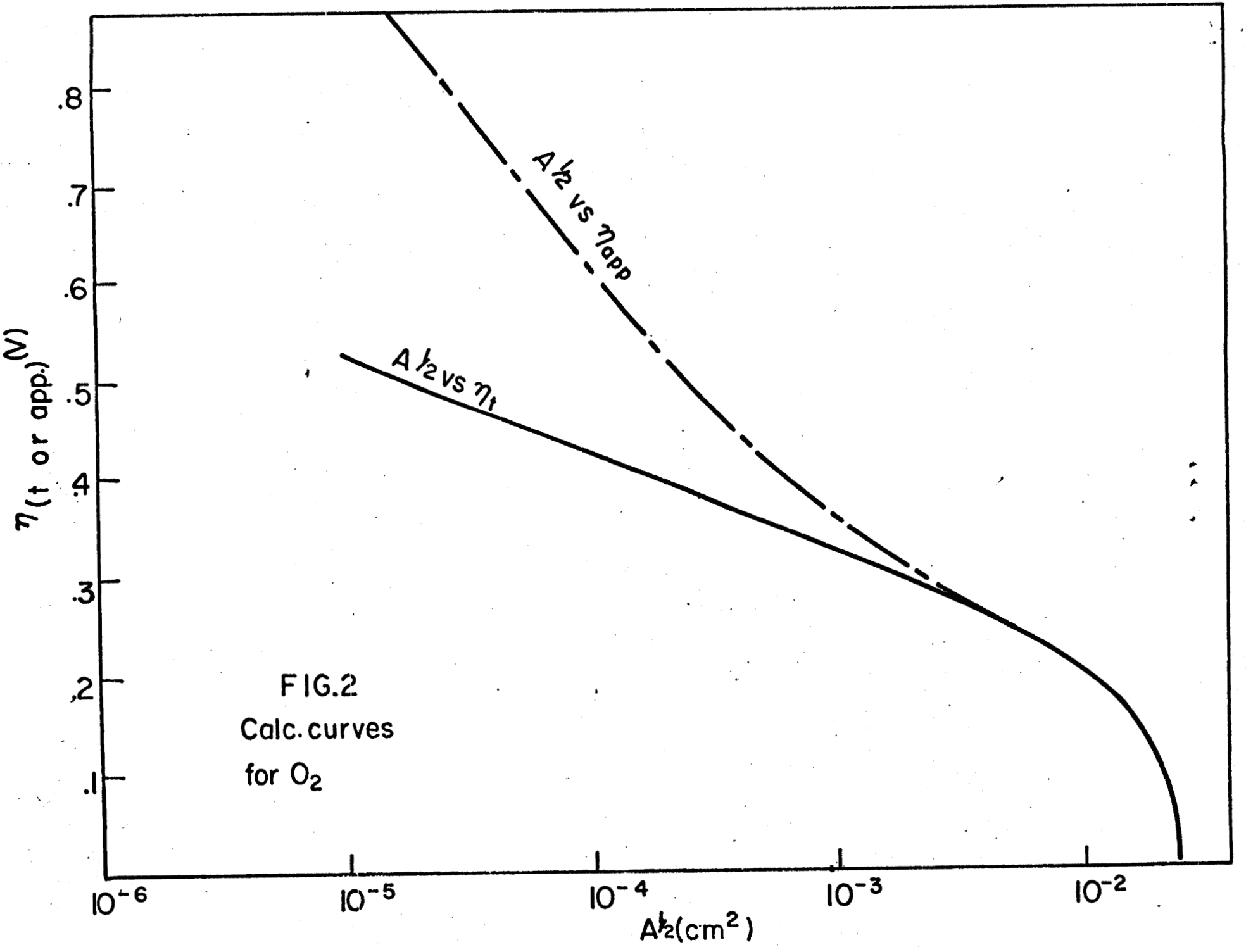

FIG.2
Calc. curves
for O_2

SECTION II. CATALYSIS OF SIMPLE ELECTRODE REACTIONS

In the last Report, results were presented for hydrogen electrode reaction on a series of alloy electrodes in the Pt-Ni system. Also were reported results of redox Fe^{+++}/Fe^{++} reaction at a number of metal and alloy electrodes (Au, Pt, Pd, Rh, Ir and Au-Pd alloys). A nearly linear relation was observed between work function and activity of different noble metals in the redox reaction. This result was unexpected as theoretical predictions suggest that the activity for a redox reaction should be independent of the electrode material. Similarly, a regular change of the activity with alloy composition was observed. Due to the importance of these results it was decided to re-examine them and to ascertain whether these results were obtained on oxide covered electrode or oxide free electrode surfaces.

To check the presence of oxides, galvanostatic charging curves were obtained on metal electrodes.

Also the nature of charge transfer was further examined, and the current-potential relations were established at different temperatures.

EXPERIMENTAL

Coverage with the oxygen containing species was determined in 1 N H_2SO_4 saturated with N_2. The usual 3 compartment cell was used for this experiment. Reference electrode was H_2 electrode separated from the test compartment by a stopcock. Care was taken to clean the electrodes and the glassware. An electrode was kept at any desired potential (from + 0.6 to + 1.5 V vs. h.e.) for a given time after which a constant

cathodic current was applied to the electrode using a fast switch. The change of potential with time was followed on an oscilloscope (535 Tektronix) and was photographed. The cathodic charging curves were obtained at regular potential intervals. To check a possible time dependence of oxide formation, an electrode was kept at a given potential for different periods of times before the cathodic charging curves were taken. A typical example would be as follows: An electrode was potentiostated at + 750 mV for 30 sec., and cathodic charging curve was taken. The procedure was then repeated but with the time of potentiostating of 1 min and 30 mins.

The amount of oxygen containing species at a given electrode was determined from the number of coulombs required to bring electrodes close to about + 0.35 V. At this potential a sharp change in V - t curves occurs. It is generally taken that at this point all oxygen is reduced and that hydrogen starts adsorbing on the electrode.

Before potentiostating each electrode was kept at about + 0.35 V for 1 min. It is previously established that at this potential all oxides of these methods are reduced in time less than 1 sec. Hence, for each coverage determination it was assured that the electrode is initially oxide free.

In another series of experiments, V - i curves were obtained on Au, Pt, Pd, Rh and Ir electrodes at 12, 27, 35, 45 and 60°C. In order to carry out experiments below or above the room temperature, an air thermostated box with a front window was used. The box was made of insulating fibre-wood. At one side of the box was a fan in front of which a

1000 watt electric coil heater was placed. Temperature of the box was maintained uniform within $\pm$ 2°C. A control type Hg-thermometer was suspended from the top of the box and was connected to the heater through a control-current supply switch. For measurements below the room temperature, a mixture of acetone-dry ice was used as the coolant placed inside the box. The actual solution temperature was measured by placing a thermometer inside the cell.

RESULTS

Coverage by oxygen containing species does change from one metal to another, and is dependent on the electrode potential. It is little affected by the time an electrode is kept at a given potential. In Table I, coverage data are collected. They are given in μ C/cm^2. Correction was made for roughness factor and charging of double layer. From previous data[2] roughness factor for Pt, Pd and Ir electrodes was taken as 1.7, and for Rh and Au electrodes as 2.

In the present experiments, i - V curves for all metals are the same as previously obtained and reported.[3]

In general, activity increased slightly with increasing temperature. In Table II, i_o's values are given for each temperature and metal examined.

In Figures 1 and 2, log i_o values are plotted vs. 1/T. Heats of activation were calculated from the slopes of these curves; they are 4.9, 5.3, 2.4, 5.5 and 7.8 kcals/mole for Pt, Ir, Pd, Au and Rh electrodes, respectively.

DISCUSSION

Coverage by oxygen containing species on Pt electrode at potentials less than 1.0 V are all below about 110 μ C/cm^2. This coverage decreases with decreasing electrode potential. At about 750 mV, which is close to the reversible Fe^{+++}/Fe^{++} electrode potential, the coverage is only 70 μC/cm^2. Similar values of coverages were previously obtained by other workers.[4] It is concluded that these coverages arise from the adsorbed oxygen species and not from oxides which can be present[4] on the electrode surface only at potentials above 1 V.

Higher coverages on Rh electrode are in agreement with previously reported values for adsorbed oxygen species.[3] Only if the electrode was potentiostated at potentials above about 1 V, oxides do form and the different types of the V - t curves are then obtained. On gold electrodes no significant coverage was detected even at electrode potentials above 1 V. An oxide forms at this electrode at potentials above about 1.2 V.

It is concluded, therefore, that all redox experiments on these metals were conducted on oxide free, bare metal electrodes. Consequently full importance should be attached to the change of activity for the Fe^{+++}/Fe^{++} redox reaction on these metals.

Low values of the activation energy, as calculated from the temperature dependence of activity, are being analyzed.

TABLE 1. COVERAGE OF O_2 ($\mu C/cm^2$) ON VARIOUS ELECTRODES AT DIFFERENT POTENTIALS

Potential V (NHE)	Time of potentiality	Pt $\mu C/cm^2$	Rh $\mu C/cm^2$	Ir $\mu C/cm^2$	Au $\mu C/cm^2$	Pd $\mu C/cm^2$
+0.6	30 sec.	----	30	----	----	----
	1 min		30			
	30 min		30			
+0.75	30 sec.	70	70	~20	~10	
	1 min	70	70	~20	~10	
	5 min					45
	30 min	70	80		~10	45
+0.900	30 sec	100	160	30**	<30*	50
	1 min	100	180	30**	<30*	50
	30 min	100	180	30**		50
+1.23	30 sec	680	----		< 40	~200
	5 min		680		< 40	300
	20 min		680	300	< 40	300
	30 m9n					
+1.5	1 min	----			400	
	5 min	----		570	400	

** + 1 V (NHE)

* + 850 (NHE)

TABLE II: VARIATION OF i_o (amp/cm^2) VALUES WITH TEMPERATURE ON DIFFERENT ELECTRODES

Electrode	12°C	27°C	35°C	45°C	60°C
Pt	6.3×10^{-3}	1.04×10^{-2}	1.32×10^{-2}	1.42×10^{-2}	2.24×10^{-2}
Rh	---	---	5.3×10^{-3}	7.5×10^{-3}	1.2×10^{-2}
Ir	4.15×10^{-3} (18°C)	2.1×10^{-3}	7.8×10^{-3}	9.5×10^{-3}	1.2×10^{-2}
Pd	1.07×10^{-2} (16°C)	1.21×10^{-2}	1.9×10^{-2}	1.5×10^{-2}	1.9×10^{-2}
Au	4.08×10^{-3}	5.5×10^{-3}	9×10^{-3}	1.14×10^{-2}	1.4×10^{-2}

REFERENCES

1. Dey and Damjanovic, Private communication.

2. Quarterly NASA Report, No. 7, 1 Oct. 1965 to 31 Dec. 1965.

3. Rao, Damjanovic, Bockris, J. Phys. Chem., 67, 2508 (1963).

4. Genshaw, Reddy and Bockris, J. Electroanal. Chem., 8, 406, 1964.

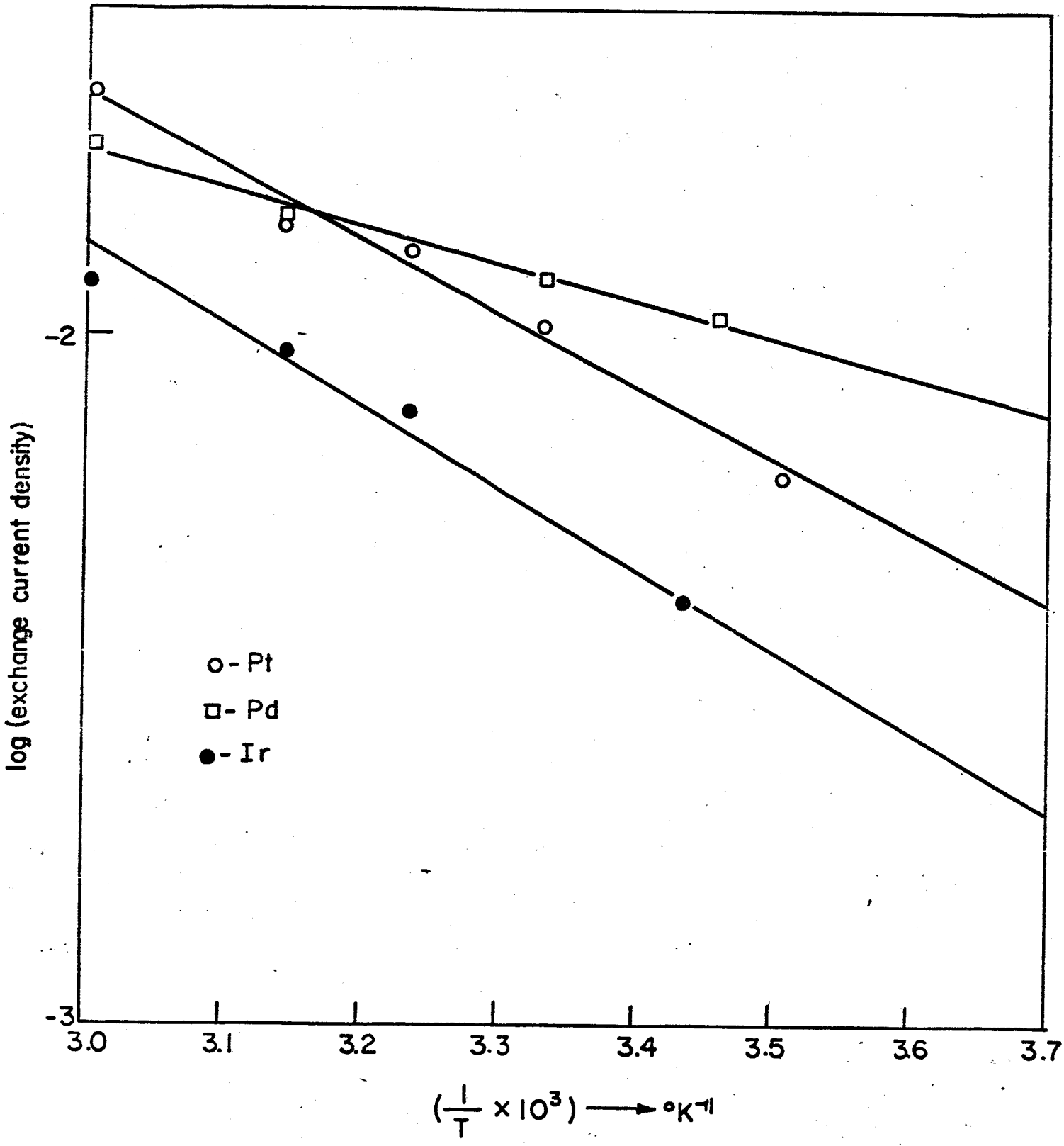
log (exchange current density)
-2
-3
o - Pt
□ - Pd
● - Ir
3.0
3.1
3.2
3.3
3.4
3.5
3.6
3.7
$(\frac{1}{T} \times 10^3) \longrightarrow {}^{\circ}K^{-1}$

FIG. 1

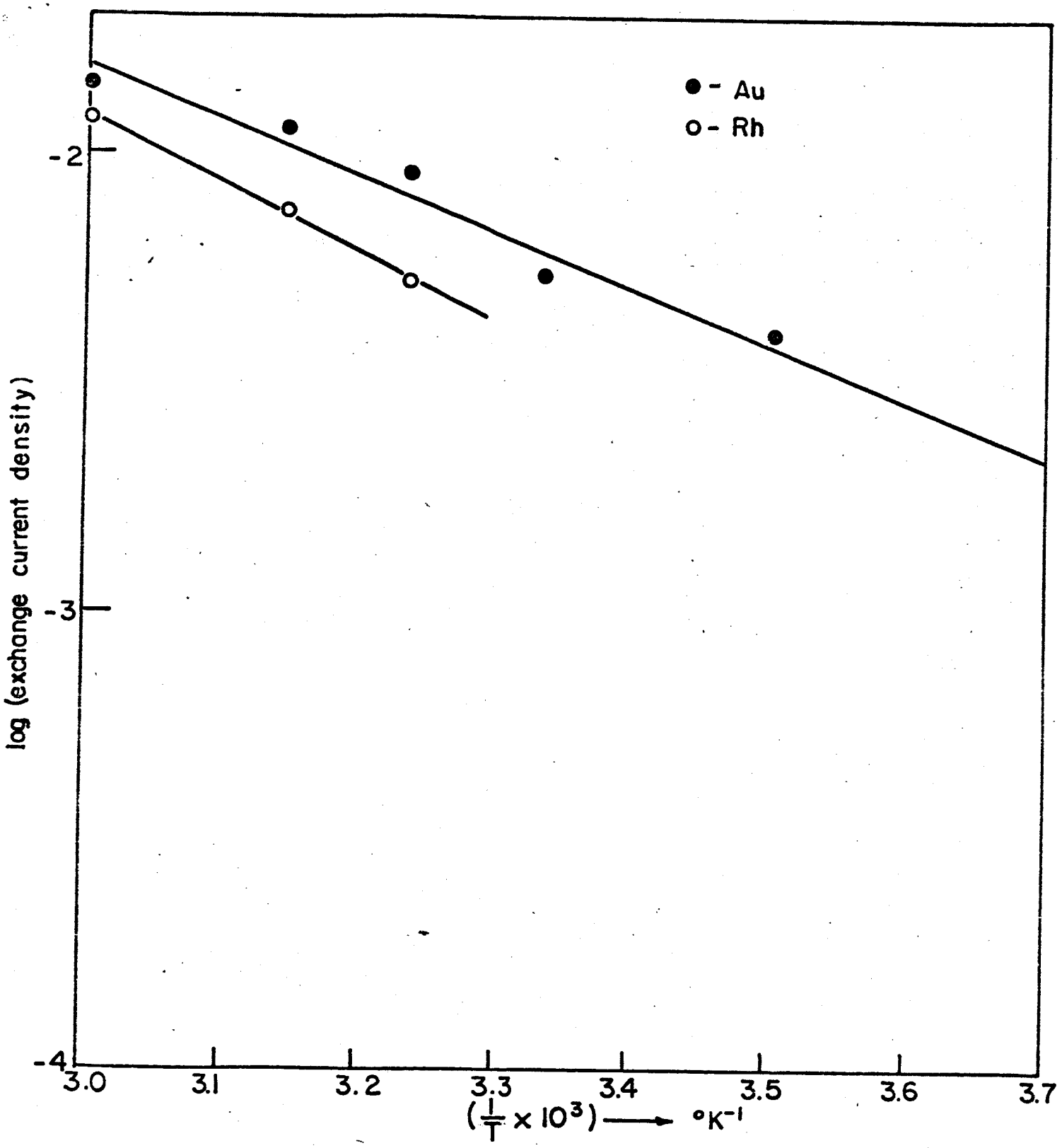
● - Au
o - Rh
-2
-3
-4
log (exchange current density)
3.0
3.1
3.2
3.3
3.4
3.5
3.6
3.7
$(\frac{1}{T} \times 10^3) \longrightarrow {}^{\circ}K^{-1}$

FIG. 2

SECTION III. POTENTIAL OF ZERO CHARGE

INTRODUCTION

Measurements of the potential of zero charge on platinum reported previously from this laboratory[1,2] have been criticized recently in a paper by Frumkin, Balashova and Kazarinov.[3] To evaluate the situation and meet the criticisms of these authors some further experiments were necessary. The main purpose of these experiments, which are reported below was to verify that the minimum in capacity observed previously in dilute solutions on Pt electrodes indeed corresponded to the potential of zero charge on this metal.

Frumkin et al.[3] claimed that in the case of platinum, the minimum in the capacitance-potential curve does not correspond to the maximum diffusivity of the double layer, and therefore to the p.z.c. Also, platinum adsorbs hydrogen and oxygen and their ionization superimposes pseudocapacity on double layer capacity. According to the above authors, the difficulties in measuring the potential of zero charge by capacitance method are not yet overcome. One has to measure the capacity at much higher frequencies so the contribution due to the pseudocapacity is negligible. The effect of pH on potential of zero charge cannot be explained on the basis of present knowledge on double layer on solid electrodes.

In the present report period, the effect of frequency and the concentration of the electrolyte on the capacitance on platinum was studied in detail in an attempt to verify our previous results.

If one has considerable variation of capacitance with frequency and the shape of the capacitance curve changes with frequency, then a pseudocapacity contribution is indicated. However, there are other factors that can cause a variation in capacitance with frequency which are as follows:

(i) Geometry of the electrode and the counter electrode assembly.

(ii) Screening of the electrode due to the presence of the glass capillary.

(iii) Penetration of the electrolyte into the space between the platinum wire and the glass surrounding it.

(iv) Roughness of the electrode (having recesses and peaks).

(v) Dielectric relaxation of the solvent effect.

Again, if the frequency is sufficiently high these effects will become smaller and contribute to the capacity measured to a lesser degree.

The variation of the electrolyte concentration gives valuable information. Firstly, as the concentration of the electrolyte is raised the diffuse layer capacity C_D is going to become larger and thus its contribution to the total capacity is smaller, which follows from the relation

$$\frac{1}{C_{measured}} = \frac{1}{C_{Helmholtz}} + \frac{1}{C_{Diffuse}} \qquad (1)$$

In dilute solutions at potentials not far away from the potential of zero charge, $C_{Diffuse}$ is small and $\frac{1}{C} \sim \frac{1}{C_{Diffuse}}$ and the measured capacity follows a cosh function with respect to charge on the electrode. Thus, one sees a minimum in the capacitance-potential curve corresponding

to the zero charge on the electrode. As the concentration is increased the contribution of the diffuse layer capacity to measured capacity becomes smaller and the minimum disappears. Secondly, if one increases the perchloric acid concentration, according to the theory of Frumkin,[3] H^+ and H being in equilibrium the contribution of pseudocapacity due to ionization of H should increase. This pseudocapacity being parallel to the double layer capacity, the negative branch of the capacity-potential curve should become steeper, as the concentration of the perchloric acid increases.

EXPERIMENTAL AND RESULTS

Apparatus and the experimentation used are described in previous reports.[2]

1. Frequency Variation of the Capacity

The high purity requirements were all the more stringent because the time required for the experiments was considerably longer. Measurements were made at various potentials increasing and decreasing the frequency. Frequencies from 500 Cps to 8000 cps were used. The transformer ratio arm bridge was calibrated for a series resistance-capacitance circuit. For this purpose General Radio Standard capacitances and resistances were used. The bridge readings were converted into series equivalent resistance (R_s) and capacitance (C_s). Proper calibration factors were applied to the readings. Then, R_s was plotted against $1/\omega$ (where $\omega = 2\pi\nu$) and R_s value for infinite frequency was obtained. The extrapolated R_s was

subtracted from the R_s readings. Now, $R_s - R_s$ (extrapolated) and C_s were back converted into a parallel equivalent resistance and capacitance. This sequence is shown in Figure 1. Figure 2 shows the capacitance-potential curves for various frequencies. Figure 3 shows C_p and R_p corrected for area of the electrode as a function of frequency on a log-log scale. If there is a considerable electrolyte penetration, the $(\partial \log R_p^{dl})/(\partial \log \nu)$ has a slope of about - 0.5 in dilute solutions and about - 1.0 in concentrated solutions. This was shown by Grantham[4] and Leikis et al.[5] considering the penetration like a transmission line. It can be seen from Fig. 4, corresponding to a situation where electrolyte penetration was known to be present that $(\partial \log R_p^{dl})/(\partial \log \nu) =$ - 0.6 and the capacitance also varies with frequency. Figure 3 has a slope of about - 1.0 and frequency dispersion of the capacitance is extremely small. This result cannot be explained very well on the basis of electrolyte penetration but can be explained on the basis of dielectric relaxation.

Thus, considering Fig. 2, it is seen that the shape of the curves does not change with frequency and therefore the pseudocapacitance contribution to the measured frequency is negligible and the minimum observed corresponds to p.z.c.

2. Variation of Electrolyte Concentration

The high purity requirements in these experiments were even higher than other experiments. The analytical grade $KClO_4$ was recrystallized several times from hot water. A stock solution of the highest

concentration possible was made and pre-electrolyzed over two days in the pre-electrolysis cell. Measurements were carried out in dilute $HClO_4$ solution first and then with successive additions of small amounts of $KClO_4$ solutions in the pre-electrolysis cell. The solution was being pre-electrolyzed under N_2 atmosphere, while the measurements were being carried out in a more dilute solution. A similar procedure was used for $HClO_4$ concentration variation.

Figure 5 shows the effect of variation of concentration of perchloric acid on the capacitance vs. potential behavior. The minimum disappears as soon as the concentration is above 5×10^{-3} N $HClO_4$. The capacitance branch on the negative side of 550 mv (r.h.e.) does not become steeper and thus gives no indication to any pseudocapacity due to ionization of H at these potentials.

In Fig. 6, the effect of variation of concentration of $KClO_4$ at constant pH on the C - V plot also shows that the minimum disappears at higher concentration and is thus characteristic of the maximum diffusivity of the double layer.

The overall change of capacitance with concentration is similar to that observed by Grahame[6] on the $Hg/HClO_4$ system.

Future Work

There is one more question as to what extent our electrodes are free of hydrogen. Thus some experiments are planned to eliminate the absorbed hydrogen by heating the platinum bead electrode at 800°C under high vacuum ($\sim 10^{-6}$ mm or better) for extended period of time (90 - 100 hours). The electrodes need to be sealed in quartz to heat them to

800°C. This type of work is in progress at the present time. Also preliminary data on silver is obtained. Capacitance measurements on silver will be carried out. Then, the apparatus for a third method will be built.

References

1. E. Gileadi, S. D. Argade and J. O'M. Bockris, J. Phys. Chem., 70, 2544 (1966).
2. Report No. 7 for the period 1 Oct. 1965 to 31 Dec. 1965, NsG-325.
3. A. Frumkin, N. Balashova and V. Kazarinov, paper presented at the symposium on electrode processes, May 1-6, 1966, Spring Meeting of the Electrochemical Society in Cleveland, Ohio.
4. D. H. Grantham, Dissertation, Iowa State University, Ames, Iowa, 1962.
5. D. I. Leikis, E. S. Sevast'yanov and L. L. Knots, Zh. Fiz. Khim., 38, 1833 (1964).
6. D. C. Grahame, Chem. Rev. 41, 441 (1947).

Captions to Figures

Fig. 1. Sequence of operations performed to obtain C_p^{dl} and R_p^{dl} from the bridge readings.

Fig. 2. Capacitance-potential plots as a function of frequency for a platinum electrode in a 10^{-3} N $HClO_4$ solution.

Fig. 3. R_p^{dl} and C_p^{dl} plotted as a function of frequency on a log-log scale, for a case when practically no penetration of electrolyte was present. -O- represent the values at - 550 mv and -x- represent values at - 500 mv.

Fig. 4. R_p^{dl} and C_p^{dl} plotted as a function of frequency on a log-log scale when electrolyte penetration was present and the slope $\partial \log R_p / \partial \log \nu = - 0.61$. C_p varies with frequency much more than Fig. 3.

Fig. 5. Capacity potential plots obtained at various concentrations of $KClO_4$ at a constant pH for the same platinum electrode.

Fig. 6. Capacity-potential curves for various concentrations of $HClO_4$ as denoted on the figure. May be noted that above 5×10^{-3} M $HClO_4$ concentration the minimum in the curve disappears and no steep rise on the negative branch of the curve as the concentration is increased.

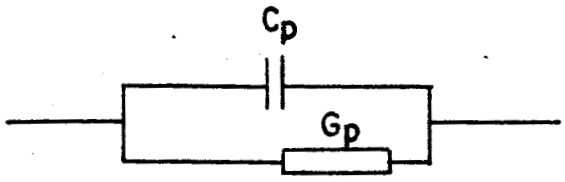

1) Parallel equivalent measured capacitance and corductance.

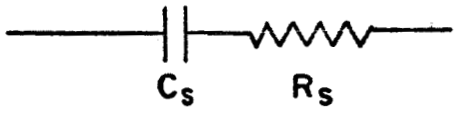

2) Conversion to series capacitance and resistance

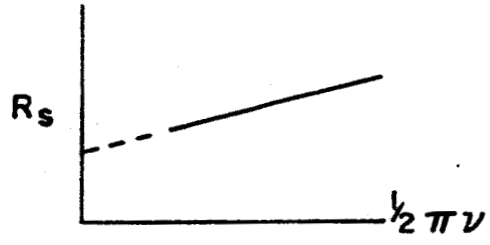

3) Extrapolate R_s to ∞ frequency - solution resistance

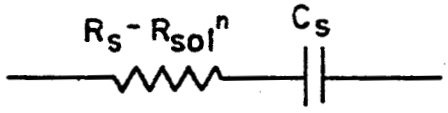

4) Subtract $R_{sol}{}^n$ from R_s

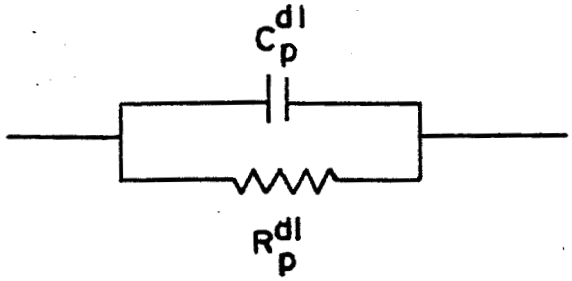

5) Back conversion of C_s and $R_s - R_{sol}{}^n$ into a parallel equivalence

Fig. 1

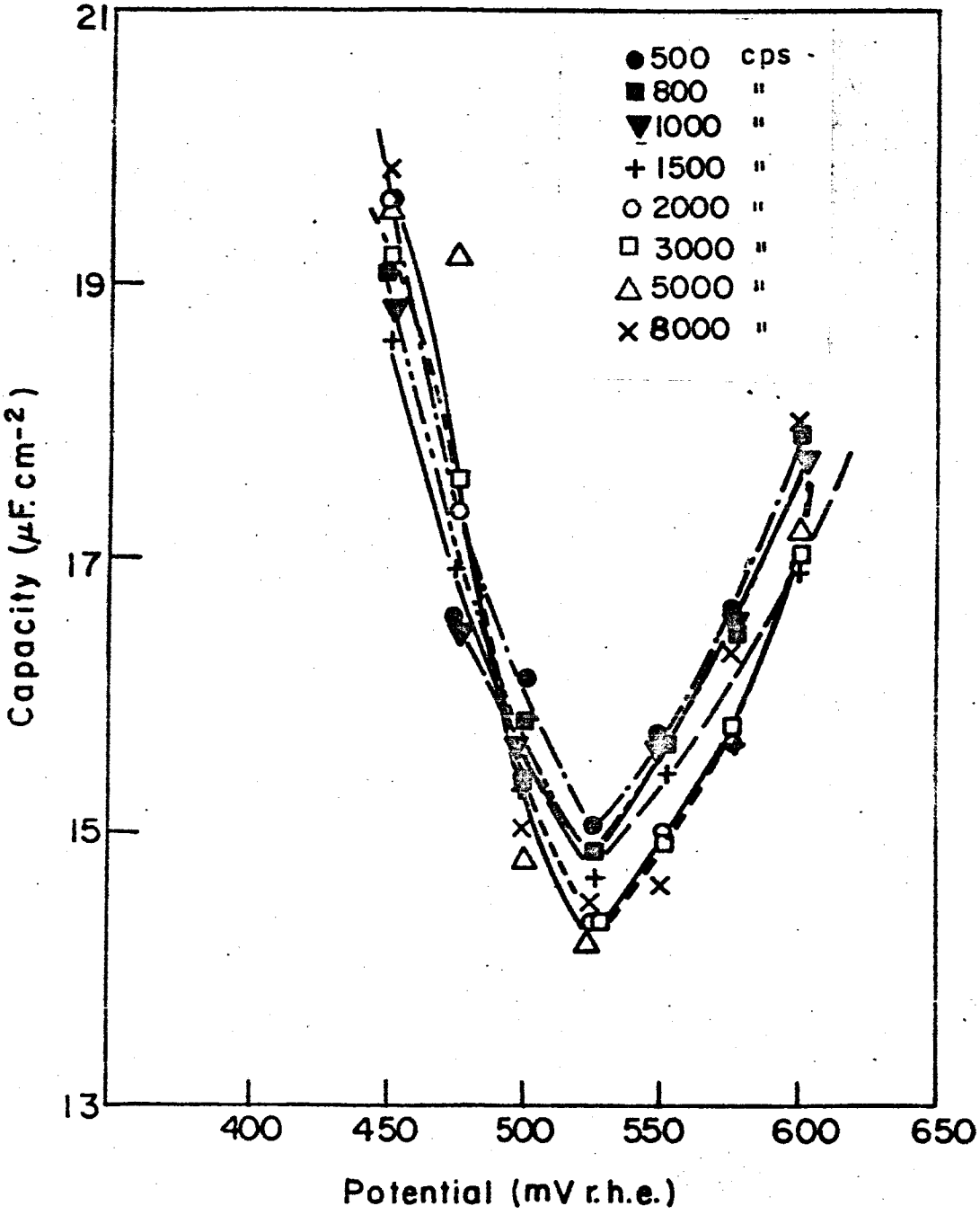

Differential capacity measurements on platinum in 0.001N $HClO_4$ solution.

FIG.2

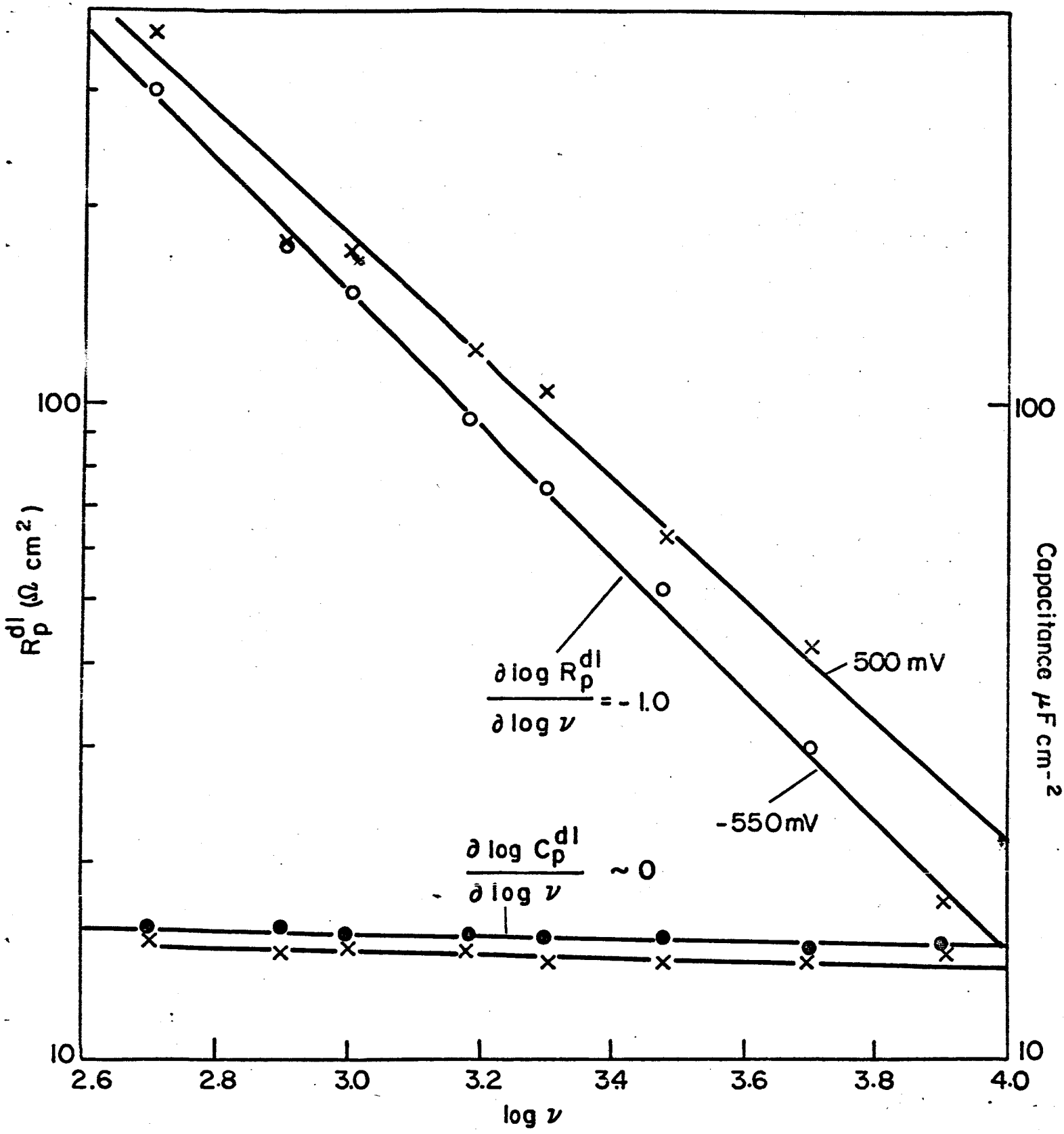

FIG. 3 Platinum electrode without electrolyte penetration.

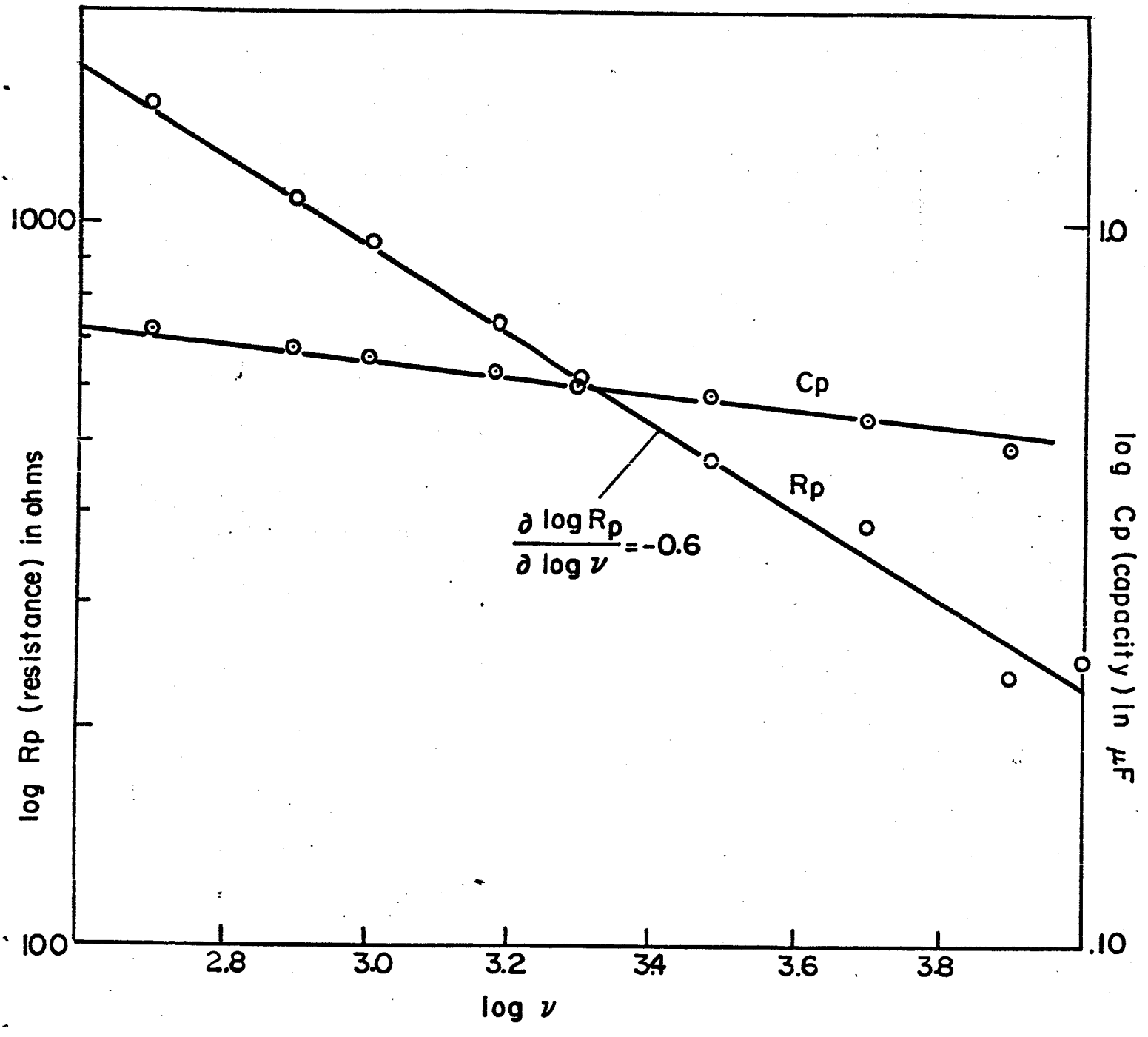

FIG.4 Platinum electrode with the presence of electrolyte penetration.

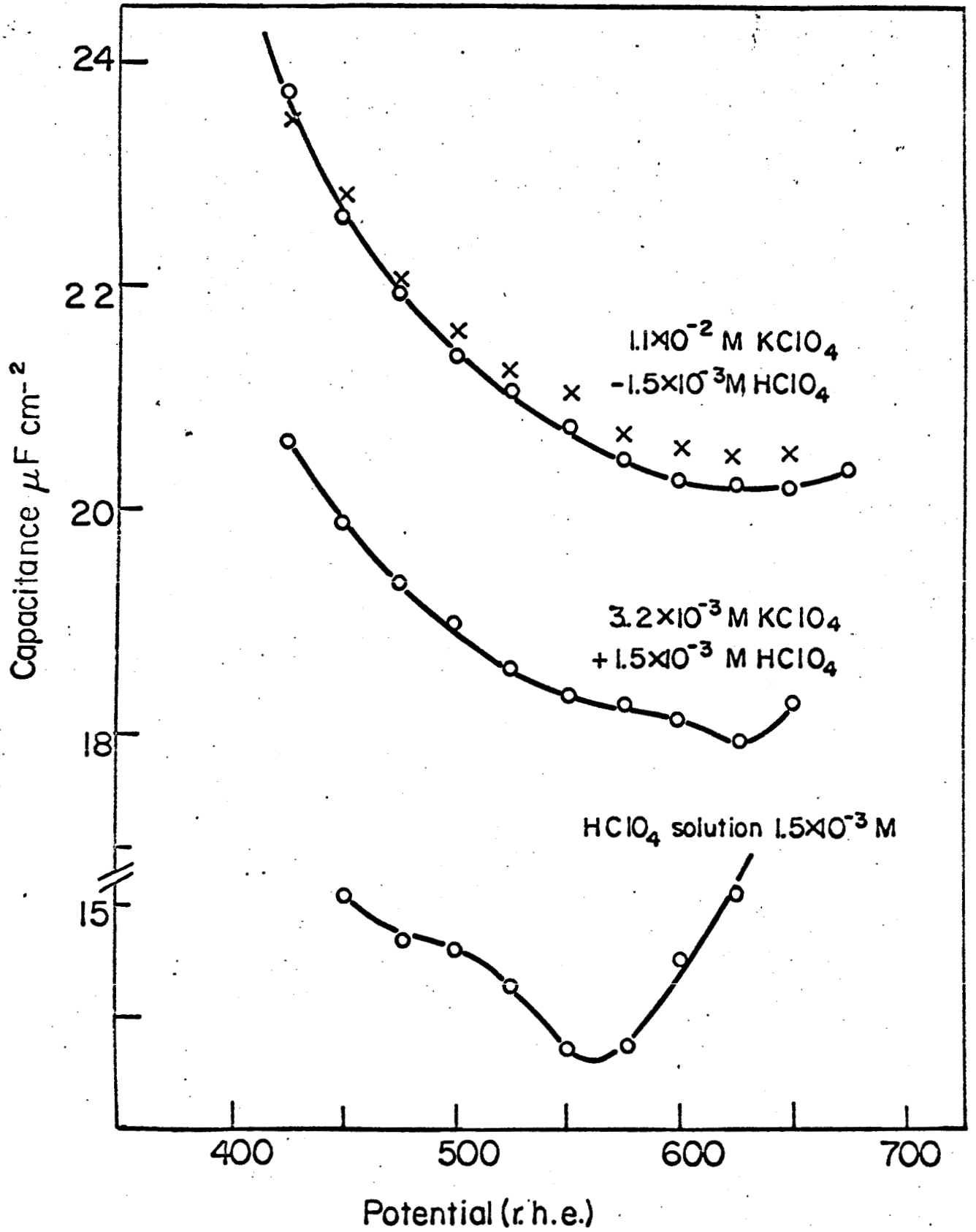
24
22
20
18
15
Capacitance μF cm⁻²
1.1×10⁻² M KClO4
-1.5×10⁻³M HClO4
3.2×10⁻³ M KClO4
+1.5×10⁻³ M HClO4
HClO4 solution 1.5×10⁻³ M
400
500
600
700
Potential (r.h.e.)

FIG.5

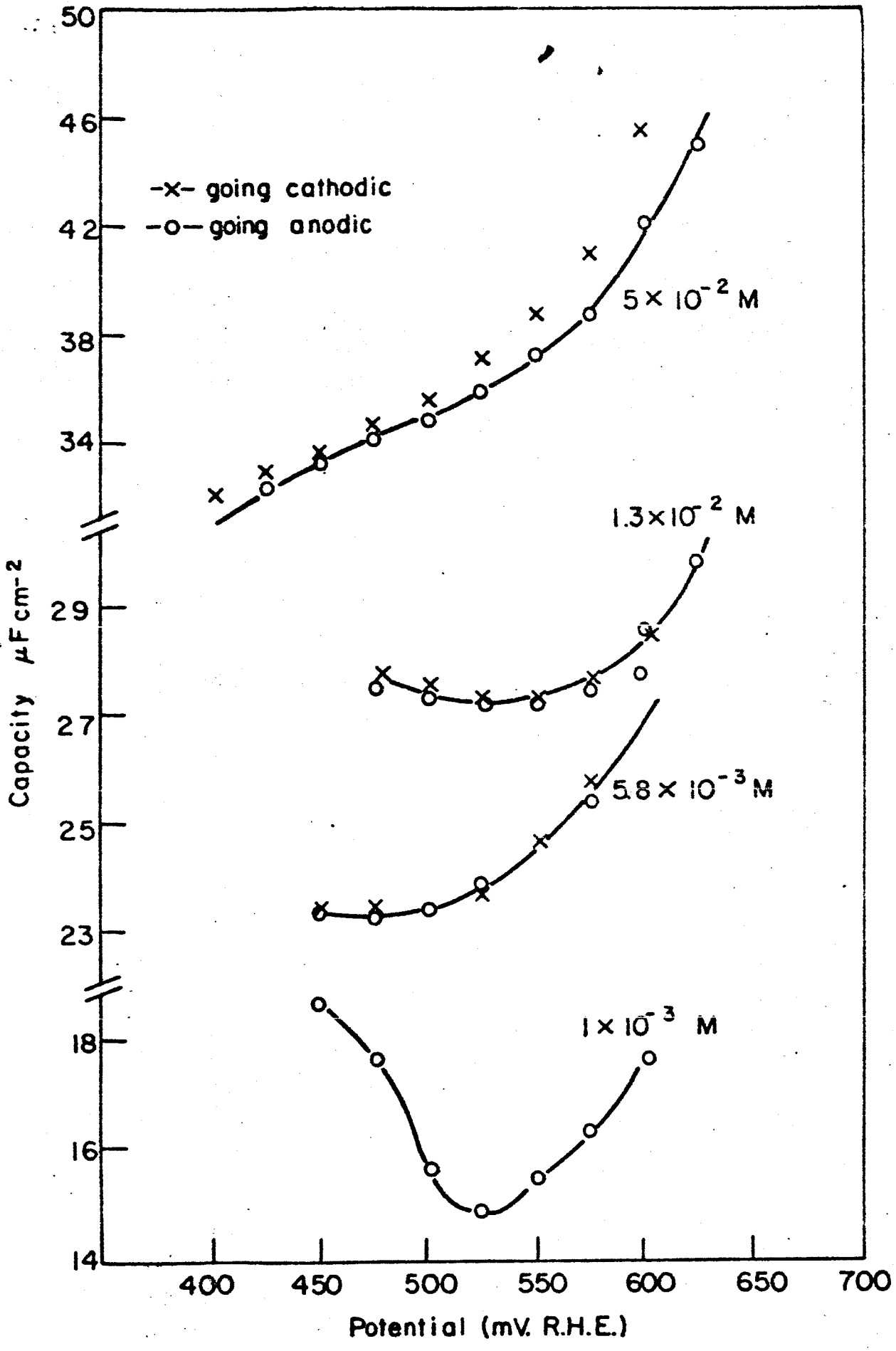
-x- going cathodic
-o- going anodic
5 × 10⁻² M
1.3 × 10⁻² M
5.8 × 10⁻³ M
1 × 10⁻³ M
Capacity μF cm⁻²
Potential (mV. R.H.E.)
50
46
42
38
34
29
27
25
23
18
16
14
400
450
500
550
600
650
700

FIG. 6

SECTION IV. ADSORPTION IN THE DOUBLE LAYER WITH SPECIFIC REFERENCE TO THERMAL EFFECTS

INTRODUCTION

In the report period experimentalwork was carried out to evaluate various methods of adsorption measurements critically. Measurements of the adsorption of benzene and ethylene by potential sweep method were continued, and in addition a study of the adsorption of benzene by galvanostatic transient method was initiated.

EXPERIMENTAL

For the potential sweep method the experimental set-up, as well as the experimental procedure were the same as previously reported,[1] except for the following modifications:

(a) Labeled benzene was used, and the bulk concentration was determined using a scintillation counter immediately after each sweep. This was done in order to avoid errors due to equilibration of benzene between the solution and gas-phase above the solution. At higher temperatures (50° and 70°) this error might become important.

(b) The amount adsorbed was calculated in a different way (see Discussion) in order to account for errors connected with various degrees of coverage with oxide in presence and in absence of organic material.

The galvanostatic transients were carried out in the same cell and on the same electrode, prepared in the same way as in the potential sweep runs.

The charging curves were obtained in blank solution and in presence of benzene. A typical example is shown in Fig. 1. The product of current and the difference between (τ_{tot} - τ_o) is taken as the amount of electricity connected with oxidation of the adsorbed benzene.

RESULTS

(a) Time dependence of adsorption

The time dependence of adsorption of ethylene and benzene was reexamined for concentrations lower than those used before. The time required to reach constant values of areas between the runs in blank solutions and adsorbate containing solutions was found to change with concentration from $\sim$ 75 min. in $\sim 10^{-7}$ m/l solution to 5 min. in $\sim 10^{-5}$ m/l solution. Adsorption time in each run was correspondingly adjusted to be longer than that required to reach steady state.

(b) Ethylene

The sweep rate used was 0.5 V/sec, measurements were carried out at 30° at the potential of 300 mV (NHE). The adsorption isotherm is shown in Fig. 2 (circles). In the same figure, results obtained by radiotracer method are shown (triangles).

In Fig. 3 the potential dependence of adsorption obtained by the sweep method is compared with that obtained by radiotracer method.

(c) Benzene, potential sweep method

The sweep rate used was 0.5 V/sec.

Adsorption isotherm obtained at 30° and 500 mV is shown in Fig. 4 (circles) along with the results of radiotracer method (triangles).

Adsorption isotherm obtained at 50° and 300 mV is shown in Fig. 5 (circles) and compared with the results of galvanostatic transients (crosses) and radiotracer method (triangles).

Adsorption isotherm at 70° shows an unusual scatter of experimental points and is still under study, as the reasons of the lack of reproducibility are not yet clear.

The potential dependence of adsorption at 50° in solution 6×10^{-6} m/l is shown in Fig. 6 (circles) and compared with the radiotracer method (triangles).

(d) Benzene, galvanostatic transient method

The amount of electricity $Q_B = i(\ _{tot} - \ _o)$ connected with the oxidation of adsorbed benzene was constant in the current density range 0.2 - 1 mA/cm^2. At higher current densities Q_B decreased. The current density used in measurements reported was 0.4 mA/cm^2. Adsorption isotherms obtained at 50° and at potential of 300 mV is shown in Fig. 5 (crosses).

Potential dependence of adsorption at 50°, as measured by galvanostatic pulse method is shown in Fig. 7 (crosses) and compared with results of radiotracer method (triangles).

DISCUSSION

1. Calculation of the amount adsorbed obtained by potential sweep method

In Fig. 8 anodic and cathodic sweeps are shown in presence and absence of benzene. For the curve corresponding to the blank solution the cathodic area (D) strictly corresponds to that of the anodic one (C). This indicates that the total amount of oxide formed during the anodic pulse is reduced during the cathodic sweep. In presence of adsorbate the cathodic area (B) is smaller than in blank solution (D). This indicates that the adsorbed organic material prevents to some degree formation of oxide. The difference in the coverage with oxide in absence and presence of the adsorbate can be then evaluated by the difference in the corresponding cathodic areas (D - B). Thus, the charge connected with oxidation of the organic material was evaluated not as a difference between the anodic areas (A - C), but as a difference between the anodic and cathodic areas obtained in the presence of the adsorbate (A - B). In this way the error connected with the change in coverage with oxide caused by adsorption of organic material was corrected.

2. Comparisons of potential sweep and radiotracer method results

The radiotracer method, being the most direct one, is assumed to give the most reliable results, which serve as reference points with which results obtained by other methods should be compared. It suffers a disadvantage that it measures the coverage not only with the adsorbate, but with the possible intermediates of the reaction the adsorbent may

undergo at the electrode. However, in the systems studied, the adsorption isotherms previously obtained showed no indications of significant amounts of other adsorbed radicals than the adsorbent itself.[2,3] The disadvantages of the potential sweep method are more numerous and were outlined previously.[4]

The results of comparison of the electrochemical methods with the radiotracer one are still ambiguous. A fairly good agreement was obtained for the ethylene system at 30°, both in the concentration and potential dependence of adsorption (Fig. 2 and 3), although in the latter one the maxima of adsorption differ by ~ 100 mV. A good agreement was also obtained for the benzene system at 50°, both with respect to concentration and potential dependence (Fig. 5 and 6). However, results obtained at 30° for benzene markedly differ from those obtained by radiotracer method.

The present results at 30° were interpreted in terms of a Frumkin isotherm:

$$\frac{\theta}{(1-\theta)} e^{r\theta/RT} = Kc$$

where $r = \frac{d(\Delta H)}{d\theta}$, ΔH is the heat of adsorption, K is the equilibrium constant. The plot of θ versus $(\log c - \log \frac{\theta}{1-\theta})$ is shown in Fig. 9. The values of r and K are respectively r = 16.7 Kcals. K = 4.2 x 10 ml/mole. The value of r differs greatly from that obtained by radiotracer method where r = 4 Kcals, whereas the equilibrium constant is of the same order of magnitude. $K_{radiot.meth.} = 2.1 \times 10^9$ ml/mole.

The discrepancy between the radiotracer method and potential sweep method results, found in benzene system at 30° and not at 50°, may

indicate that the agreement at the latter temperature is fortuitous. However, no final conclusions can be drawn before the results obtained at 70°C are obtained, and a few other systems are investigated.

3. Comparison of results of galvanostatic and potential sweep method

In Fig. 5 the adsorption isotherms obtained by the two methods are shown. The agreement is very good, as would indeed be expected. If the potential sweep results are not corrected for the difference in the amount of oxide formed in presence and absence of the adsorbate (cf. Section IV.1), the integration of the trace obtained by anodic potential sweep leads to the anodic charging curve that would be obtained under the same conditions, as shown below. In the potential sweep method dV/dt is constant, thus multiplying the current axis by dt/dV a plot of $idt/dV = dq/dV$ versus potential is obtained.

In the galvanostatic pulse method, the time axis can be multiplied by the value of constant current resulting in a plot of $it = q$ versus potential.

In Fig. 10 the integrated values of q obtained from the potential sweep method for blank (crosses) and benzene containing (circles) solutions are shown together with the directly obtained oscillograms of charging curves (lines 'a' and 'b'), in which the time axis was multiplied by the value of current. The agreement is excellent, proving experimentally the equivalency of both methods.

It must be mentioned, however, that both methods are expected to be equivalent only in this range of current densities applied in the

galvanostatic pulse method, which results in a $\Delta V/\Delta t$ value during the transient between the two given potentials approximately equal to dV/dt value in the potential sweep. At too high or too low current densities the same deviations may be expected as those arising from too high or too low sweep rates.

References

1. Quarterly Progress Report No. 7 (1 Oct. 1965 to 31 Dec. 1965), NsG325.
2. E. Gileadi, B. T. Rubin and J. O'M. Bockris, J. Phys. Chem., 69, 3335 (1965).
3. W. Heiland, E. Gileadi and J. O'M. Bockris, J. Phys. Chem., 70, 1207 (1966).
4. S. Srinivasan and E. Gileadi, Electrochem. Acta, 11, 321 (1966)

Fig 1. Typical anodic charging curve obtained in blank solution (a), with superimposed curve in presence of benzene (b).

Fig 2. Adsorption isotherm for ethylene obtained at 30° C. Circles: potential sweep method ($\Delta V/\Delta t$ = 0.5 V/sec, potential of adsorption 0.3 V); triangles: radiotracer method (potential of adsorption 0.4 V).

Fig 3. Potential dependence of ethylene adsorption at 30° C. Circles: potential sweep method; triangles: radiotracer method.

Fig 4. Adsorption isotherm for benzene obtained at 30° C and 0.5 V. Circles: P.S.M.; triangles: radiotracer method.

Fig 5. Adsorption isotherm for benzene obtained at 50° C and 0.3 V. Circles: P.S.M.; crosses: galvonostatic method; triangles: radiotracer method.

Fig 6. Potential dependence of benzene adsorption at 50° C. Comparison between P.S.M. (circles) and radiotracer method (triangles) concentration of benzene 6×10^{-6} M.

Fig 7. Potential dependence of adsorption obtained at 50° C for benzene by galvanostatic method (crosses) and radiotracer method (triangles) concentration of benzene 11×10^{-7}M.

Fig 8. Typical curves obtained by potential sweep in presence (- - -) and absence (———) of hydrocarbons.

Fig 9. The plot θ versus $(\lg c - \lg \frac{\theta}{1-\theta})$ for benzene isotherm at 30° C.

Fig 10. Integrated curves obtained in anodic part of potential sweep (Fig 8).

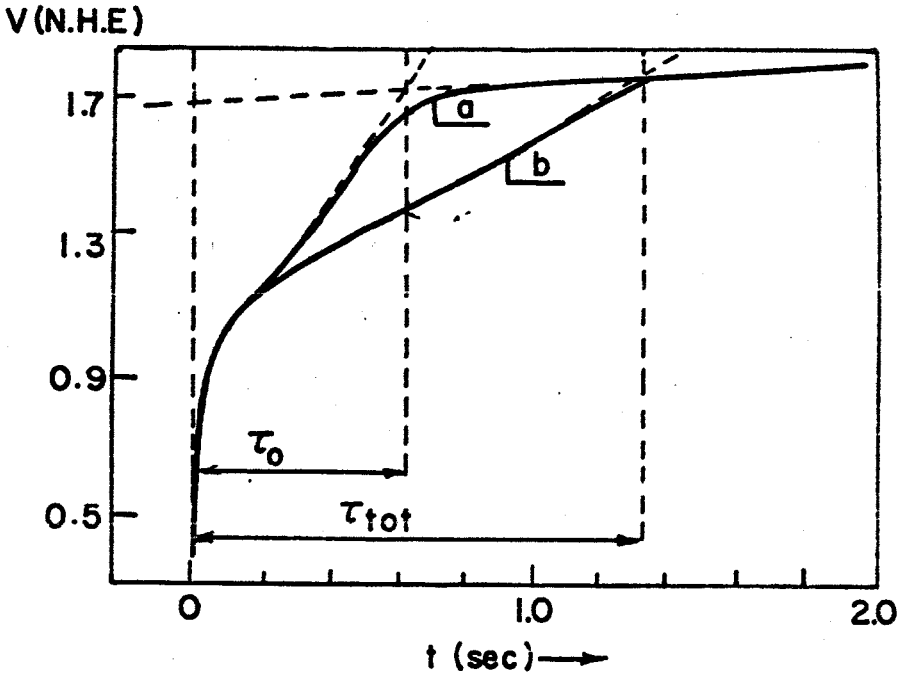

FIG. 1 Typical anodic charging curve
a-blank solution (saturated with nitrogen)
b-in presence of benzene.

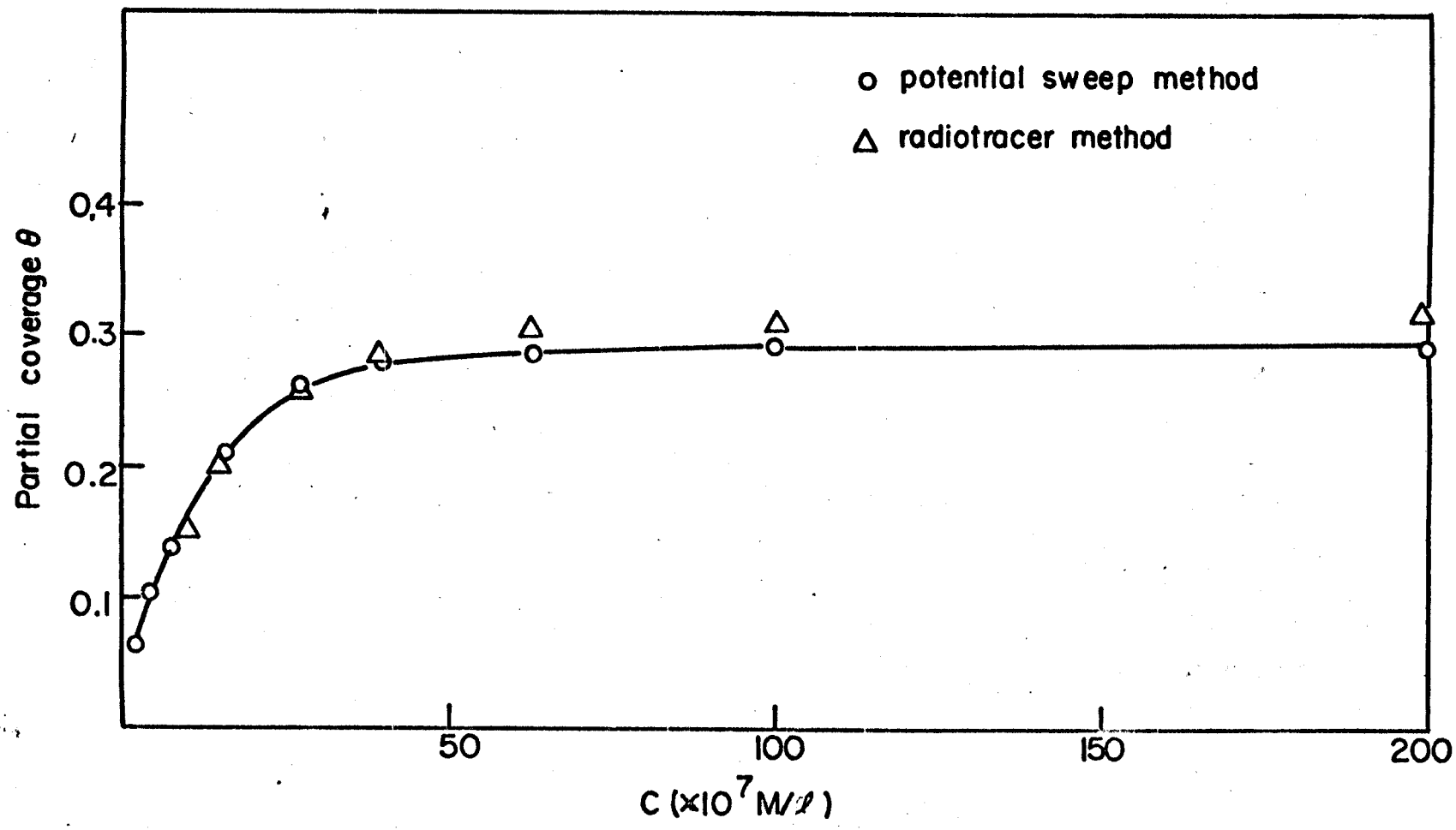
o potential sweep method
△ radiotracer method
Partial coverage θ
0.4
0.3
0.2
0.1
50
100
150
200
C (×10⁷ M/ℓ)

FIG. 2

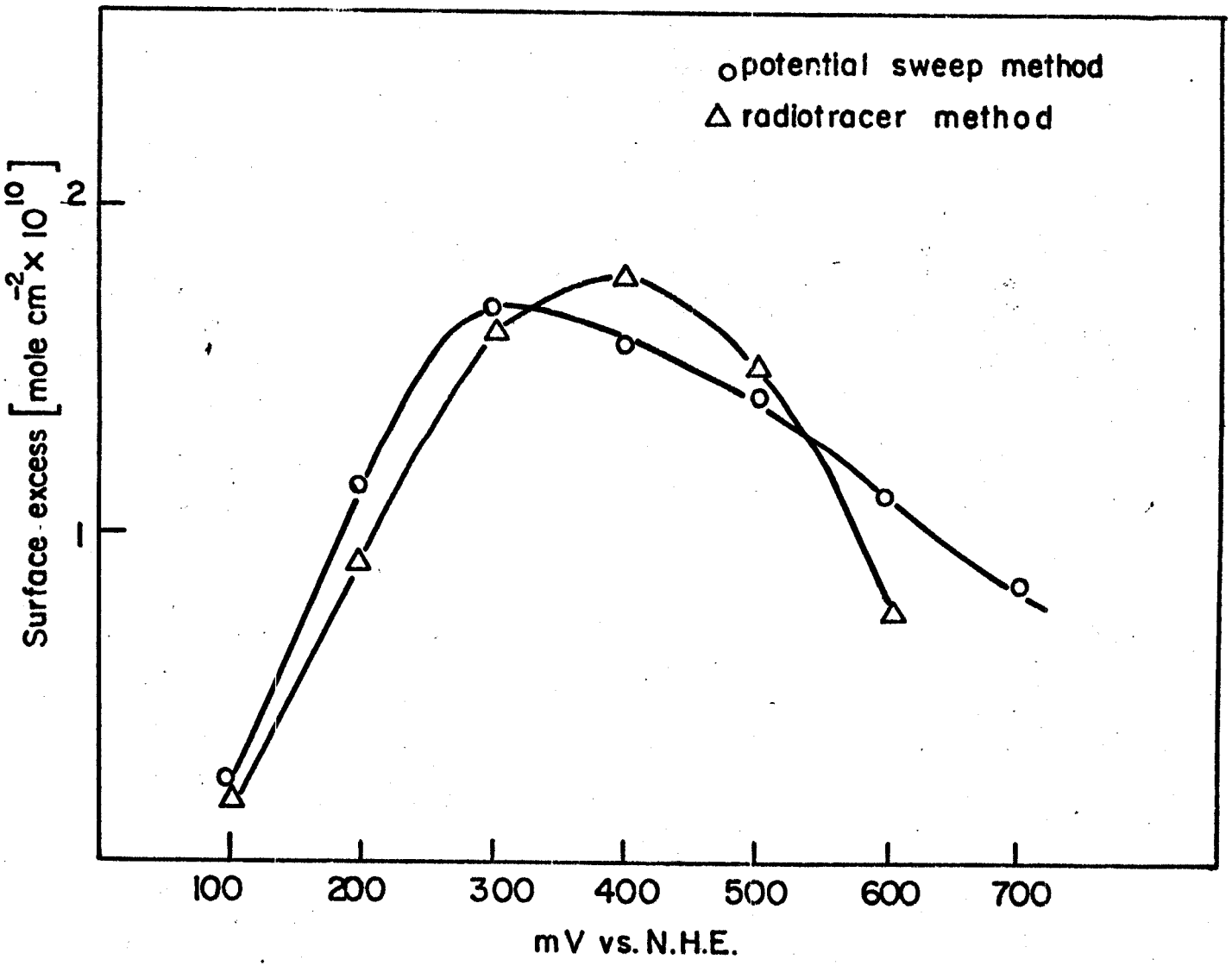
o potential sweep method
Δ radiotracer method
Surface excess [mole cm^{-2} × 10^{10}]
2
1
100
200
300
400
500
600
700
mV vs. N.H.E.

FIG. 3.

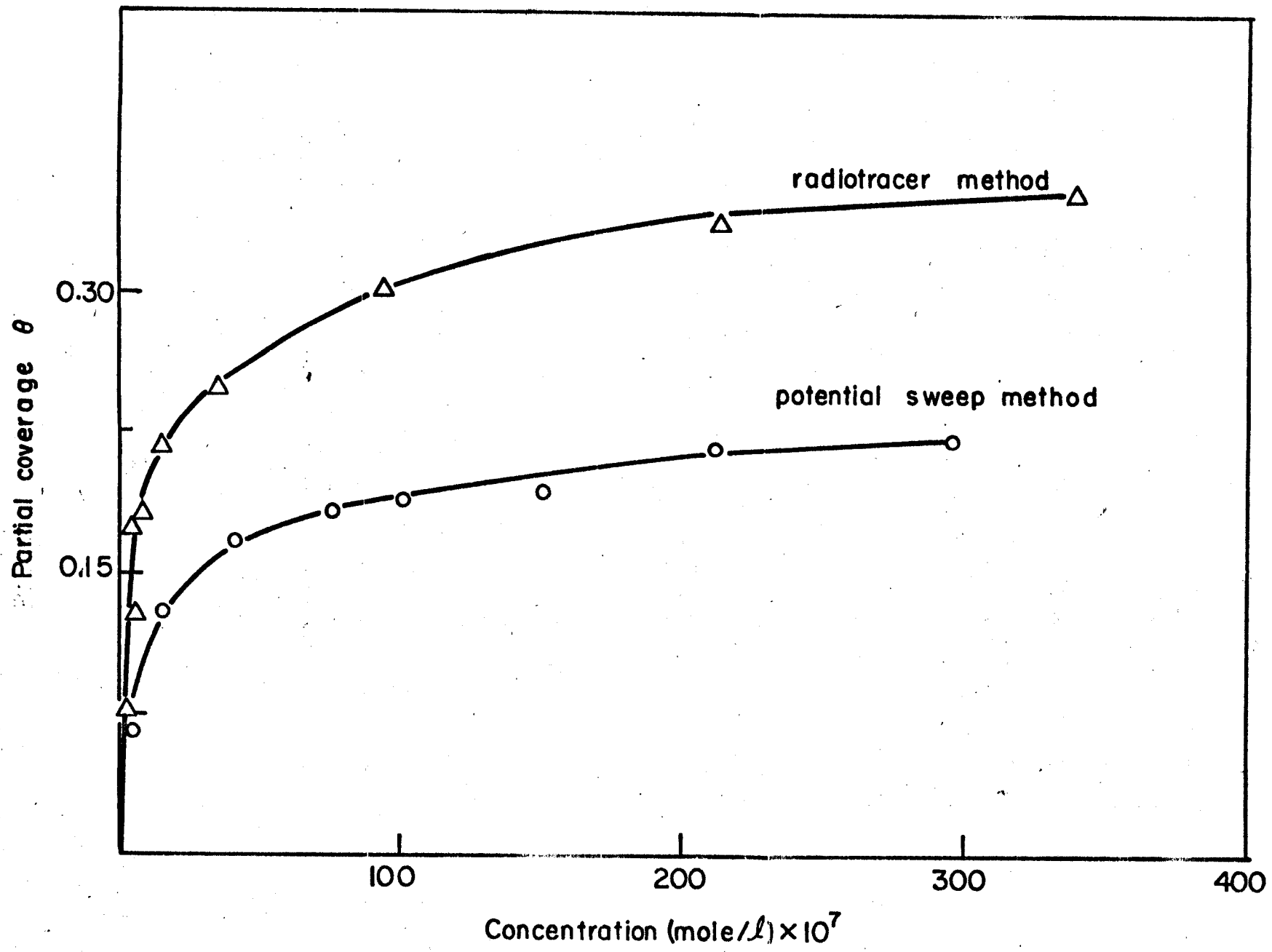
radiotracer method
potential sweep method
0.30
0.15
Partial coverage θ
100
200
300
400
Concentration (mole/ℓ) × 10⁷

FIG. 4

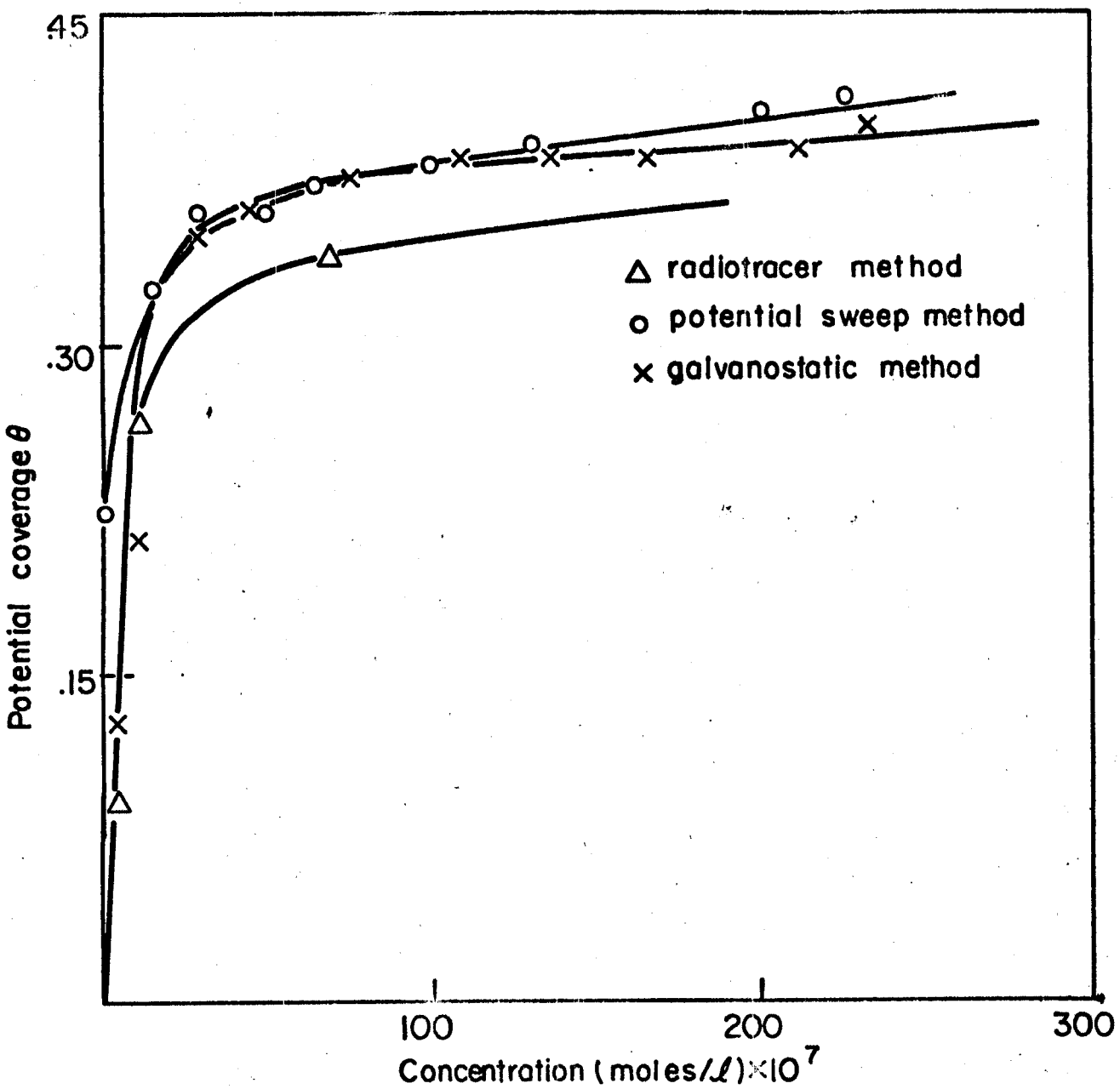
.45
.30
.15
Potential coverage θ
△ radiotracer method
o potential sweep method
× galvanostatic method
100
200
300
Concentration (moles/ℓ)×10⁷

FIG. 5

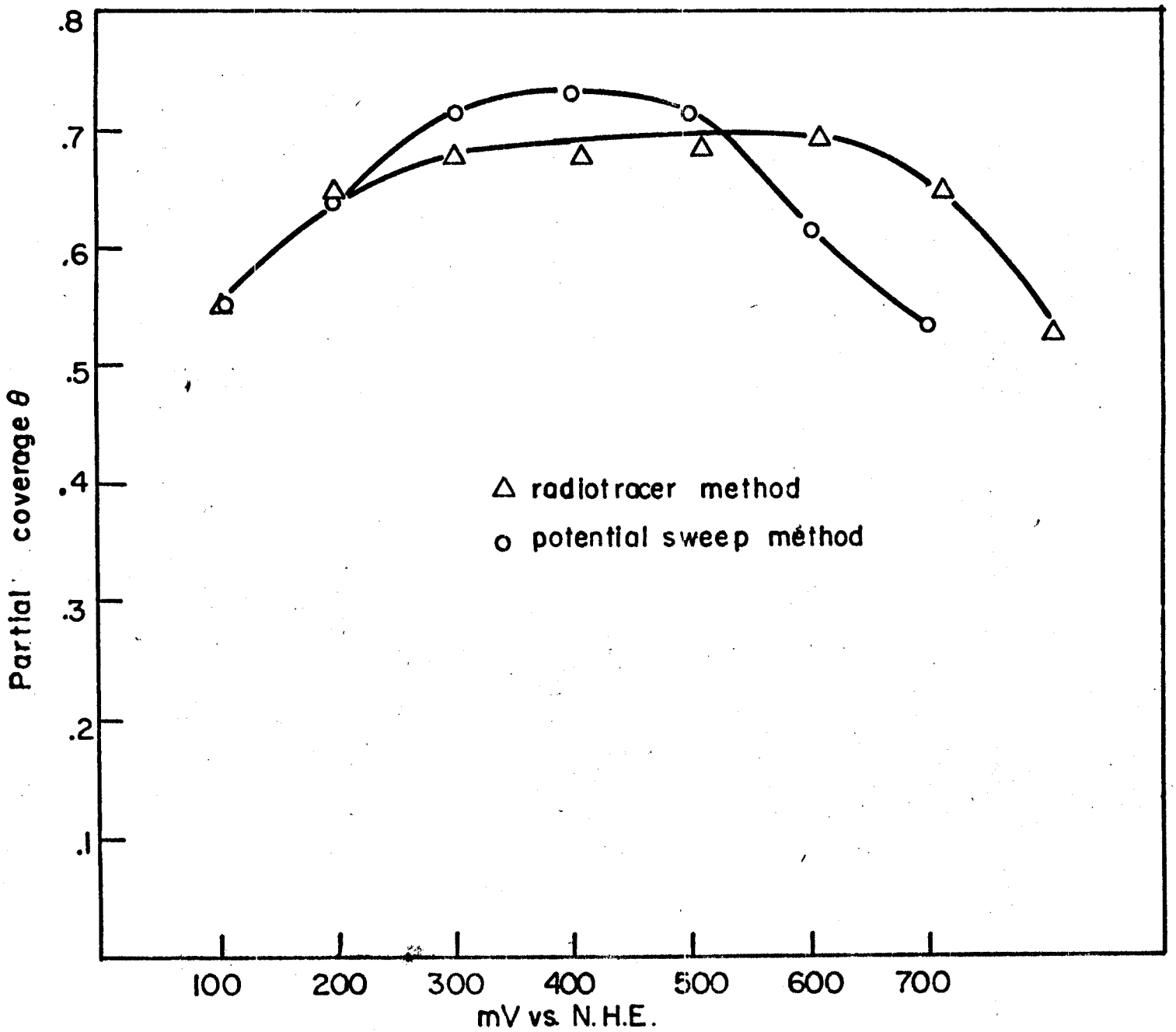
.8
.7
.6
.5
.4
.3
.2
.1
Partial coverage θ
△ radiotracer method
o potential sweep method
100
200
300
400
500
600
700
mV vs. N.H.E.

FIG. 6

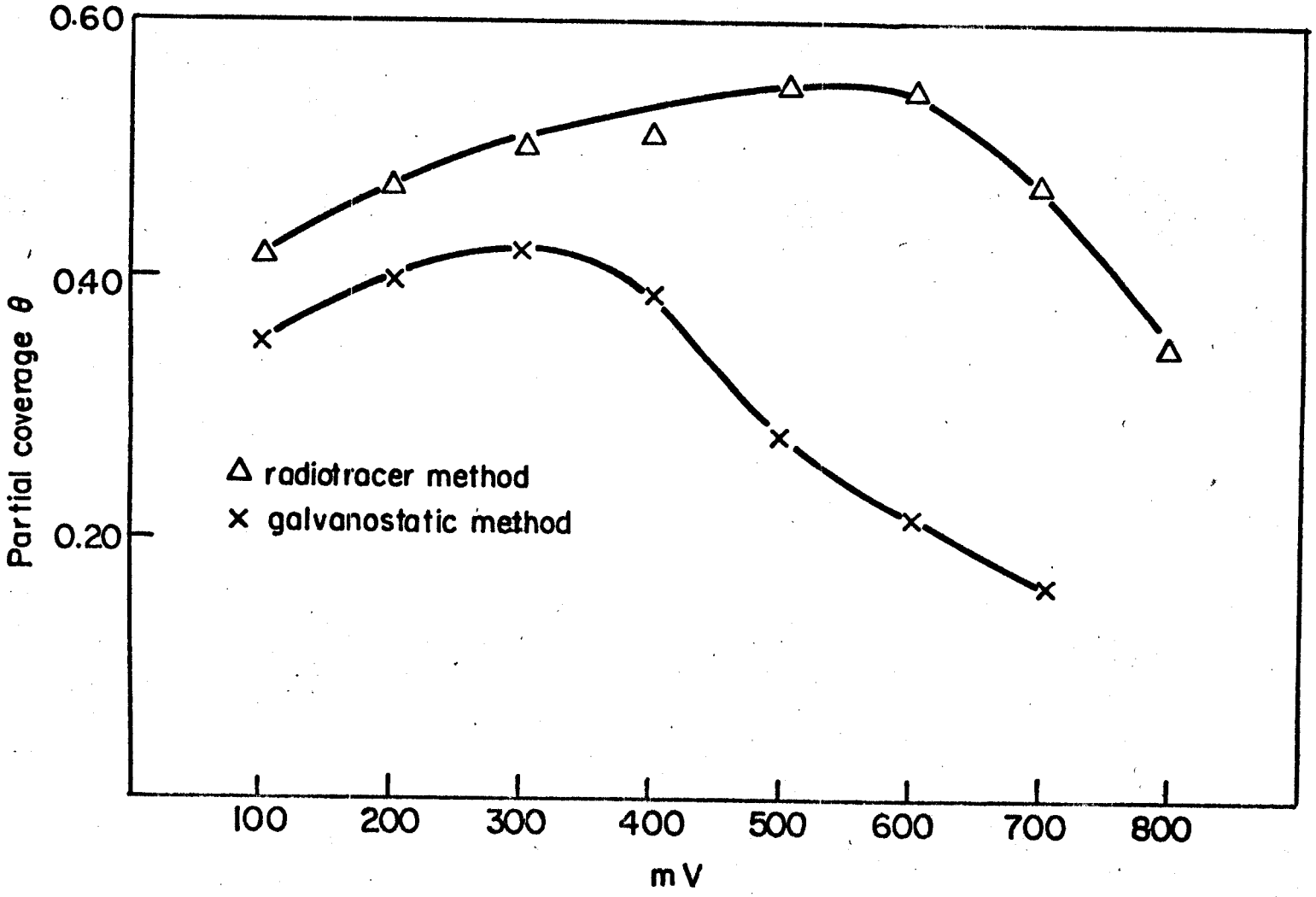
0.60
0.40
0.20
Partial coverage θ
Δ radiotracer method
× galvanostatic method
100
200
300
400
500
600
700
800
mV

FIG.7

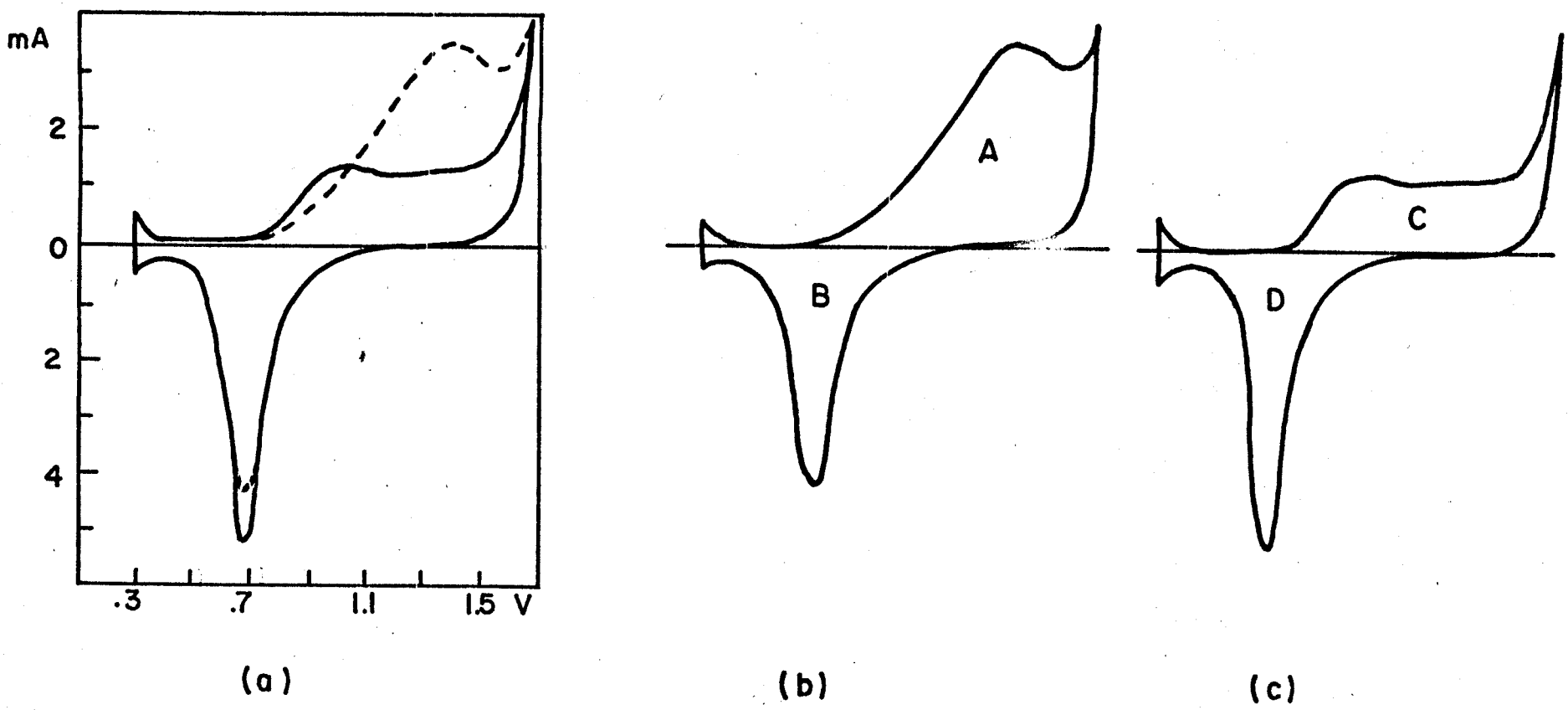

FIG.8 Typical curve obtained by potential sweep method.
(a) curve obtained in blank solution (——) with superimposed curve in presence of hydrocarbons (- - -)
(b) curve obtained in presence of hydrocarbons.
(c) curve obtained for blank solution.

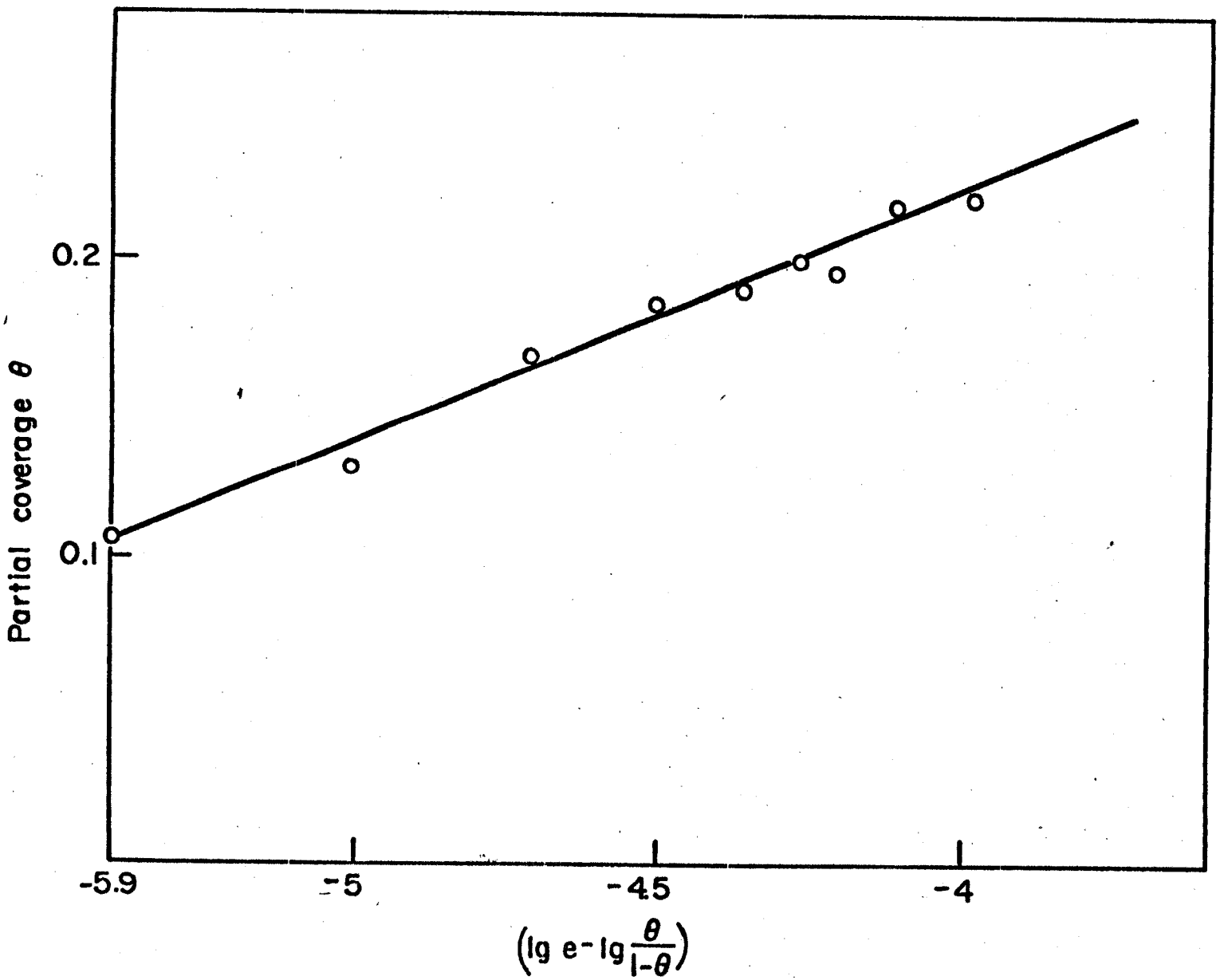
0.2
0.1
Partial coverage θ
-5.9
-5
-4.5
-4
$\left(\lg e - \lg \frac{\theta}{1-\theta}\right)$

FIG.9

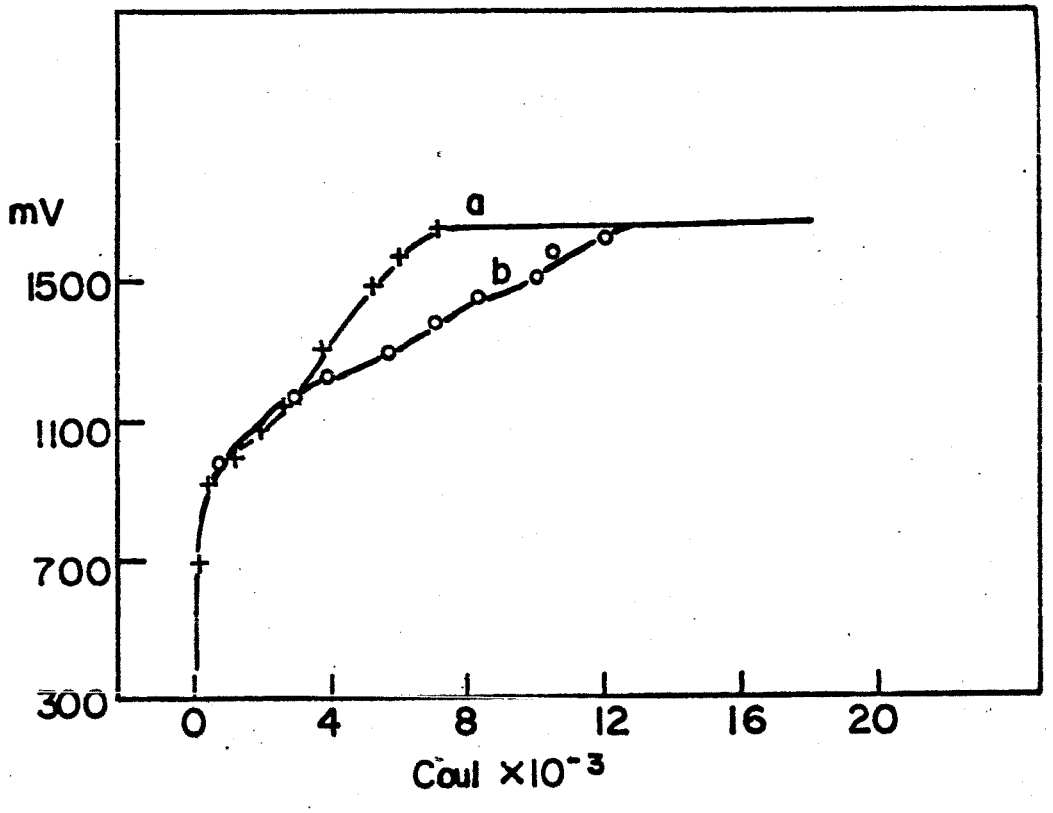

FIG. 10

SECTION V. ELECTRODE KINETIC ASPECTS OF ELECTROCHEMICAL ENERGY CONVERSION

During this period, a theoretical analysis of the thin film model of porous gas diffusion electrodes was made. The abstract of this work is found in the Appendix attached to this report.

In addition, a chapter entitled "Electrochemical Techniques in Fuel Cell Research" was written in collaboration with Dr. E. Gileadi. This Chapter will appear in the Hand Book of Fuel Cell Technology, which is being edited by C. Berger. In this chapter, the methodology of investigation is first treated. It is followed by a section which deals with the principles of electrode kinetics in the investigation of mechanisms of reactions. This section treats the theory behind (i) determination of the overall reaction, (ii) diagnostic criteria for determination of the reaction path, (iii) role of electrosorption. In the next section the experimental methods for these determinations are broadly divided under (i) steady state measurements, (ii) transient measurements, (iii) electrosorption measurements, (iv) detection and identification of intermediates, (v) determination of adsorption pseudocapacitance. Finally, a section on studies on porous electrodes is dealt with. Here, after briefly discussing the overpotential-current density and current distribution relations, the topics of (i) important parameters determining the performance of porous electrodes, (ii) methods of preparation of porous electrodes, (iii) physical methods of characterization of porous electrodes, (iv) electrochemical measurements on porous electrodes and (v) model pore studies are treated.

SECTION VI. PUBLICATIONS UNDER GRANT NsG-325

1. Forces involved in the Specific Adsorption of Ions on metals from aqueous solution, J. O'M. Bockris and T. Anderson, Electrochimica Acta, 9, 347 (1964).

2. Electrochemical Kinetics of Parallel Reactions, E. Gileadi and S. Srinivasan, J. of Electroanal. Chem., 7 (1964) 452-457.

3. Electrocatalysis, J. O'M. Bockris and H. Wroblowa, J. Electroanal. Chem., 7 (1964) 428-451.

4. Basis of possible continuous self activation in an electrochemical energy converter, J. O'M. Bockris, B. J. Piersma, E. Gileadi and B. D. Cahan, J. Electroanal. Chem., 7 (1964) 487-490.

5. Ellipsometry in Electrochemical Studies, A. K. N. Reddy and J. O'M. Bockris, U. S. Dept. Comm. Natl. Bureau of Standards, Misc. Publication 256, Sept. 15, 1964, 229-244.

6. Ellipsometric Study of oxygen-containing films on Platinum electrodes. A. K. N. Reddy, M. Genshaw and J. O'M. Bockris, J. Electroanal. Chem., 8 (1964) 406-407.

7. Ellipsometric Determination of the Film Thickness and Conductivity during the Passivation Process on Nickel, A. K. N. Reddy, M. G. B. Rao and J. O'M. Bockris, J. Chem. Phys., 42, 6, 2246-2248, 15 March 1965.

8. A Brief Outline of Electrocatalysis, J. O'M. Bockris and S. Srinivasan, 19th Annual Proceedings Power Sources Conference, May 1965.

9. Proton Transfer across Double Layers, J. O'M. Bockris, S. Srinivasan, and D. B. Matthews, Disc. Faraday Soc., 1965, No. 39.

10. The Potential of Zero Charge on Pt and its pH Dependence, E. Gileadi, S. D. Argade and J. O'M. Bockris, J. Phys. Chem., 1966, Vol. 70, 2044.

11. The Potential Sweep Method: A Theoretical Analysis, S. Srinivasan and E. Gileadi, Electrochim. Acta, 11, (1966) 321-335.

12. Electrode Kinetic Aspects of Electrochemical Energy Conversion, J. O'M. Bockris and S. Srinivasan, J. Electroanal. Chem. 11 (1966) 350-389.

The following are in course of publication

13. An ellipsometric study of oxide films on platinum in acid solutions, J. O'M. Bockris, A. K. N. Reddy and M. Genshaw.

14. Electrocatalysis in Ethylene Oxidation, A. Kuhn, H. Wroblowa and J. O'M. Bockris.

15. Electrosorption, edited by E. Gileadi, Plenum Press.

16. Theory of Porous Gas Diffusion Electrodes Using the Thin Film Model, S. Srinivasan and H. D. Hurwitz, Electrochem. Acta.

17. Chapter on Electrochemical Techniques in Fuel Cell Research, to be published in Handbook on Fuel Cell Technology, edited by C. Berger, Prentice Hall.

SECTION VII. APPENDIX

ABSTRACT

All forms of polarization losses are considered. It is not possible to obtain analytic solutions for the apparent current density-overpotential and current distribution relations under these conditions. Analytic solutions are, however, possible for some special cases: viz. activation-ohmic and concentration-ohmic.

Numerical calculations are carried out in the case where all forms of polarization are present, varying the kinetic and physical parameters. This model yields higher current densities than the simple pore model under identical conditions. The general shapes of the curves are similar for the two models. A region of normal Tafel slope is followed by a region of double this slope at higher over-potentials which then passes over into the limiting current region. The current distribution relations show a special type of behavior. At low over-potentials, there is uniform current distribution, followed by increasing uneven distribution but close to the limiting current, it again passes over into a region of uniform current distribution.

Numerical calculations for the current and potential distribution in the case of only activation and ohmic polarization are presented in a simplified manner in terms of a parameter which contains all the kinetic and physical quantities. For this case, the apparent current density is slightly lower than that for the simple pore model at high over-potentials.

SECTION VII. APPENDIX

THEORY OF POROUS GAS DIFFUSION ELECTRODES USING THE THIN FILM MODEL

S. Srinivasan and H. D. Hurwitz*

1. Introduction

The present paper deals with an analysis of porous gas diffusion electrodes for the thin film model. The model was first considered assuming that activation processes are fast and that the rate is controlled by mass transfer and ohmic processes.[1,2] The subsequent treatments of this model do not show clearly the influence of kinetic parameters on the overall rate as a function of overpotential and on the current distribution problems.[3,4] In the present work, a numerical method is used in the case where all forms of polarization are present to ascertain these effects. In addition, some limiting cases are considered - case of only activation and ohmic polarization, case of only concentration and ohmic polarization - where analytic solutions are possible for the current density as a function of the overpotential and the current generated as a function of distance in the film.

2. Description of model and reaction sequence

In the thin film model, the basic assumption is that a thin

---

*On leave of absence from the Free University of Brussels, Brussels, Belgium.

film of liquid exists above the meniscus and is in contact with the solid phase in the pore (Fig. 1). It is assumed that the thickness of the film, Δr, is a constant and is given by

$$\Delta r = r_2 - r_1 \tag{1}$$

where r_2 and r_1 are distances of the electrode-electrolyte and electrolyte gas interfaces from the z axis - a cylindrical coordinate system is used as in a preceding paper. Since Δr is small compared to the radius of the pore, r_2, it is assumed that the film forms a right angle edge with the meniscus of the electrolyte. It is further assumed that all the current is generated on the electrode surface in the film region (i.e., from $z = 0$ to $z = \ell$ in Fig. 1).

A reaction sequence of the following type is assumed for this model.

(i) Diffusion of reactant gas, R, from outer end of porous electrode, A, at which gas pressure is P^o to gas-electrolyte interface.

(ii) Dissolution of R in electrolyte at gas electrolyte interface $r = r_1$ for $0 \leqslant z \leqslant \ell$.

(iii) Radial diffusion of the dissolved gas from $r = r_1$ to $r = r_2$ for $0 \leqslant z \leqslant \ell$.

(iv) Electrosorption of dissolved reactant gas at electrode (R_{ads}).

(v) Charge transfer reaction of R_{ads} to give R^+_{ads}.

(vi) Charge transfer reaction of R^+_{ads} to give products, P.

(vii) Diffusion of products away from the electrode and migration of ions through film.

These steps may be represented by

$$R_g \longrightarrow R_{g,e} \qquad \text{I}$$

$$R_{g,e} \longrightarrow R_{s,e} \qquad \text{II}$$

$$R_{s,e} \longrightarrow R_{s,m} \qquad \text{III}$$

$$R_{s,m} \longrightarrow R_{ads} \qquad \text{IV}$$

$$R_{ads} \longrightarrow R^{+}_{ads} + e^{-}_{o} \qquad \text{V}$$

$$R^{+}_{ads} \longrightarrow P_{s,m} + (n-1)e^{-}_{o} \qquad \text{VI}$$

$$P_{s,m} \longrightarrow P_{s,e} \qquad \text{VII}$$

It is assumed that step V is the activation controlling intermediate step at the electrode. All the other charge transfer steps at the electrode are assumed to be fast and are grouped under VI. The hydrogen and oxygen dissolution reactions serve as examples of this type of reaction. It is also assumed that concentration polarization is caused only by a change of the reactant concentration at the electrode-electrolyte interface (m). The symbols R_g and R_s represent the reactant R in the gaseous state and in solution; e stands for the gas electrolyte interface.

In a previous paper,[5] it was shown that the rates of the first two steps - viz. diffusion of reactant gas through the electrolyte free part of the pore and its dissolution in the electrolyte at the gas-electrolyte interface are considerably faster than the subsequent steps of the overall reaction. The limiting currents due to these processes were found to be of the order of 10^3 and 10^5 amp cm^{-2} respectively, using a pore radius of 10^{-4} cm.

3. Theoretical analysis of model

3.1 Case where all forms of polarization are present

The rate of the electrode reaction in an element dz of the electrode (Fig. 1) is given by

$$dI = 2\pi r_2 \, dz \, i_o \left[\frac{c}{c^o} (r_2,z) \exp(\eta F/2RT) - \exp(-\eta F/2RT) \right] \qquad (2)$$

where i_o is the exchange current density of the electrode reaction when the concentration at the electrode is c^o. η is the sum of activation and concentration overpotentials. The symmetry factor, β, is assumed to be 1/2.

The average potential drop in the element, dz, is expressed by

$$d\eta = I \frac{dz}{\kappa \pi (r_2^2 - r_1^2)} \qquad (3)$$

where κ is the specific conductivity of the electrolyte. In order that the concentration, $c(r_2,z)$, at the electrode surface in the steady state be ascertained one may assume that the reactant gas has a flux only in the r direction and has the equilibrium concentration, c^o, at the gas-electrolyte interface along the film. Since the reattant is only consumed at the electrode surface,

$$dI = - 2\pi r \, dz \cdot DnF \, (\partial c/\partial r) \qquad (4)$$

Integrating equation (4) using the boundary condition that at $r = r_1$

$$c = c^o \qquad (5)$$

$$c(r_2,z) = c^o + \frac{1}{2\pi DnF}\left(\frac{dI}{dz}\right) \ln\left(\frac{r_1}{r_2}\right) \tag{6}$$

Using equation (6) in (2)

$$\frac{dI}{dz} = 2\pi r_2 i_o\left[\left(1 + \frac{1}{2\pi DnFc^o}\left(\frac{dI}{dz}\right) \ln\frac{r_1}{r_2}\right)\exp(\eta F/2RT) - \exp(\eta F/2RT)\right] \tag{7}$$

Equation (7) may be rewritten in the form

$$\frac{dI}{dz} = \frac{4\pi r_2 i_o \sinh(\eta F/2RT)}{1 + \frac{r_2 i_o}{DnFc^o} \ln\left(\frac{r_2}{r_1}\right) \exp(\eta F/2RT)} \tag{8}$$

Differentiating Equation (3) with respect to z and combining the resulting equation with Equation (8)

$$\frac{d^2\eta}{dz^2} = \frac{\left[4r_2 i_o/\kappa(r_2^2 - r_1^2)\right] \sinh(\eta F/2RT)}{1 + \frac{r_2 i_o}{DnFc^o} \ln\left(\frac{r_2}{r_1}\right) \exp(\eta F/2RT)} \tag{9}$$

The above differential equation may be converted into an analogous one but with dimensionless parameters, making the substitutions

$$(\eta F/2RT) = y \tag{10}$$

and

$$z/\ell = x \tag{11}$$

Thus, Equation (9) reduces to

$$\frac{d^2y}{dx^2} = \frac{a \sinh y}{1 + b \exp y} \tag{12}$$

where

$$a = \frac{2r_2 i_o \ell^2 F}{\kappa RT(r_2^2 - r_1^2)} \tag{13}$$

and

$$b = \frac{r_2 i_o}{DnFc^o} \ln\left(\frac{r_2}{r_1}\right) \tag{14}$$

In terms of the dimensionless parameters, the current at z is given by

$$I_z = 2\kappa\pi(r_2^2 - r_1^2)\,(RT/\ell F)(dy/dx)_{x=x} \tag{15}$$

and the total current by

$$I_t = 2\kappa\pi(r_2^2 - r_1^2)(RT/\ell F)(dy/dx)_{x=1} \tag{16}$$

The ratio of the current at z to the total current (at $z = \ell$) is thus

$$\frac{I_z}{I_t} = \left(\frac{dy}{dx}\right)_{x=x} \Big/ \left(\frac{dy}{dx}\right)_{x=1} \tag{17}$$

It is not possible to solve Equation (12) analytically. A numerical solution is, therefore, necessary to study the influence of the various parameters ($i_o, \kappa, D, c^o, r_2, r_1, \eta$) on the $I_z - z$ and $I_t - \eta_\ell$ ($\eta = \eta_\ell$ at $z = \ell$) relations.

A first integration of Equation (12), however, is possible using the substitution

$$(d^2y)/(dx^2) = (1/2)(d/dy)(dy/dx)^2 \tag{18}$$

the boundary condition that when $\eta = \eta_o$ (i.e., $y = y_o$)

$$d\eta/dz = 0 \text{ (i.e., } dy/dx = 0) \tag{19}$$

and the substitution $u = \exp y$ (20)

The solution is

$$\left(\frac{dy}{dx}\right)^2 = a\left[\exp(-y) - \exp(-y_o) + b(y - y_o) + \frac{1 - b^2}{b} \ln\left(\frac{1 + b \exp y}{1 + b \exp y_o}\right)\right] \tag{21}$$

Combining Equations (17) and (21), the expression for the current distribution within the film is obtained as a function of y (or η). In order that y many be expressed as a function of x, it is necessary to integrate Equation (21) with the boundary condition that at

$$x = 0 \text{ (i.e., } z = 0), \qquad y = y_o \text{ (i.e., } \eta = \eta_o) \tag{22}$$

Analytic solutions for some limiting cases of Equation (12) are possible which will be considered in the following sections.

3.2 Case of activation and ohmic polarization

When concentration polarization is absent $b \exp y << 1$ in Equation (12). This case corresponds to that of activation-ohmic control. Under these conditions, Equation (12) becomes

$$d^2y/dx^2 = a \sinh y \tag{23}$$

Using the boundary condition (19) a first integration of Equation (23) yields

$$(dy/dx)^2 = 2a\left[\cosh y - \cosh y_o\right] \tag{24}$$

This equation may be integrated by making the substitutions

$$k = \frac{1}{\cosh (y_o/2)} = \sin \theta \tag{25}$$

and

$$\cos \psi = \frac{\sinh (y_o/2)}{\sinh (y/2)} \tag{26}$$

Using this method and the boundary condition (22), the solution to Equation (24) is

$$k \cdot F(k,\psi) = a^{1/2} x \tag{27}$$

where

$$F(k,\psi) = \int_o^x \frac{d\psi}{(1 - k^2 \sin^2\psi)^{1/2}} \tag{28}$$

$F(k,\psi)$ is the elliptic integral of the first kind and tables of this integral of the first kind are available as a function of θ and ψ. (dy/dx) may be expressed in terms of the variable ψ by using Equation (26) in (24). Thus,

$$dy/dx = (4a)^{1/2} \sinh (y_o/2) \cdot \tan \psi \tag{29}$$

Using Equation (29) in (15), the current is expressed as a function of ψ (or x through Equation (27)). The ratio of the current at $x = x$ to that at $x = 1$, is thus

$$\frac{I_z}{I_t} = \frac{\tan(\psi)_{x=x}}{\tan(\psi)_{x=1}} \tag{30}$$

and $$I_t = \chi \pi (r_2^2 - r_1^2) (2RT/\ell(F)(4a)^{1/2} \sinh(y_o/2) \tan(\psi)_{x=1} \tag{31}$$

Some special cases may now be considered.

(i) Conditions when $(y - y_o) < 0.15$, Equation (23) may be rewritten as

$$\frac{d^2y}{dx^2} = a \sinh\left[(y - y_o) + y_o\right]$$

$$= a\left[\sinh (y-y_o) \cosh y_o + \cosh (y-y_o) \sinh y_o\right] \qquad (32)$$

Since $(y - y_o)$ is small, the above equatinn may be reduced to

$$\frac{d^2y}{dx^2} = a\left[(y - y_o) \cosh y_o + \sinh y_o\right] \qquad (33)$$

Equation (33) can be solved analytically by making the substitution

$$u = (y - y_o) + \tanh y_o$$

and using the boundary conditions (18) and (19) which results in the solution

$$(y - y_o) + \tanh y_o = \tanh y_o \cosh (K_1 x) \qquad (34)$$

where $$K_1^2 = a \cosh y_o \qquad (35)$$

Differentiating Equation (34)

$$\frac{dy}{dx} = K_1 \tanh y_o \sinh (K_1 x) \qquad (36)$$

Using Equation (35) in (17) the ratio of the current at z to the total current (at $z = \ell$) is given by

$$\frac{I_z}{I_t} = \frac{\sinh (K_1 x)}{\sinh K_1} \qquad (37)$$

This relation shows that the ratio I_z/I_t varies $\sinh K_1 x$ and

$$I_t = \chi \pi (r_2^2 - r_1^2) \frac{2RT}{\ell F} K_1 \tanh y_o \sinh K_1 \qquad (38)$$

If $K_1 << 1$, (which corresponds to a low i_o, low η_o, high χ, a high $\Delta r = r_2 - r_1$) Equation (34) reduces to

$$(y - y_o) + \tanh y_o = \tanh y_o \left[1 + \frac{K_1^2 x^2}{2}\right] \tag{39}$$

i.e. $$y - y_o = \frac{a}{2} \sinh y_o \cdot x^2 \tag{40}$$

and Equation (36) becomes

$$dy/dx = K_1^2 \tanh y_o \, x$$
$$= a \sinh y_o \, x \tag{41}$$

Under these conditions, (I_z/I_t) is given by

$$I_z/I_t = x \tag{42}$$

and $$I_t = \pi (r_2^2 - r_1^2) \frac{2RT}{\ell F} a \sinh y_o \tag{43}$$

According to this relation, there is a linear variation of the current with distance and the observed Tafel slope would be the normal one. Further, if y_o is itself small, Equations (40) and (41) become

$$(y - y_o) = (a/2) \cdot y_o \, x^2 \tag{44}$$

and $$dy/dx = a \, y_o \, x \tag{45}$$

A linear variation of current with distance means that there is a uniform generation of current in the pore from z = 0 to z = ℓ. For this case, the change in potential from z = 0 to z = ℓ is small and at any z, this change is proportional to the square of the distance.

For the case in which y_o is large but $(y - y_o)$ is small, the total current (I_t) - potential (η_ℓ) relation is Tafellian. However, if y_o is small (0.2), a linear I_t - η_ℓ relation would be obtained.

(ii) Conditions under which y_o is large ($y_o > 2.30$)

With these conditions, Equation (23) reduces to

$$\frac{d^2y}{dx^2} = \frac{a}{2} \exp y \tag{46}$$

Integrating Equation (46), using the boundary condition (19)

$$\left(\frac{dy}{dx}\right)^2 = a\left[\exp y - \exp y_o\right]$$
$$= a\,(\exp y_o)\left[\exp(y - y_o) - 1\right] \tag{47}$$

Using the substitution

$$u^2 = \left[\exp\,(y - y_o) - 1\right] \tag{48}$$

and the boundary condition (22), Equation (47) may be integrated to yield the solution

$$\tan^{-1}\left[\exp(y - y_o) - 1\right]^{1/2} = \frac{a^{1/2}}{2} \cdot \exp(y_o/2) \cdot x \tag{49}$$

Equation (49) may also be expressed in the form

$$(y - y_o) = 2 \ln \sec\left[(a^{1/2}/2)\, \exp(y_o/2) \cdot x\right] \tag{50}$$

The latter expression gives the variation of potential with distance in the film. Introducing Equation (49) into (47)

$$dy/dx = a^{1/2}\, \exp(y_o/2)\, \tan\left[(a^{1/2}/2)\, \exp\,(y_o/2) \cdot x\right] \tag{51}$$

The above equation gives the variation of current with distance in the thin film. Using Equation (50) in (17)

$$\frac{I_z}{I_t} = \frac{\tan\left[(a^{1/2}/2)\, \exp\,(y_o/2) \cdot x\right]}{\tan\left[(a^{1/2}/2)\, \exp(y_o/2)\right]} \tag{52}$$

and

$$I_t = \gamma\{\pi (r_2^2 - r_1^2) \frac{2RT}{\gamma F} a^{1/2} \exp(y_o/2) \tan\left[(a^{1/2}/2) \exp(y_o/2)\right] \quad (53)$$

A limiting case is when

$$(a^{1/2}/2) \exp (y_o/2) \leq 1 \quad (54)$$

(i.e., low i_o, high γ, high Δr). Under these conditions,

$$\tan\left[(a^{1/2}/2) \exp(y_o/2)\ x\right] \simeq (a^{1/2}/2) \exp(y_o/2)x \quad (55)$$

and

$$\sec\left[(a^{1/2}/2) \exp (y_o/2)x\right] \simeq 1 \quad (56)$$

Using these approximations in Equations (49) to (52)

$$y - y_o \simeq 0 \quad (57)$$

$$(dy/dx) = (a/2) \exp (y_o) \cdot x \quad (58)$$

and

$$I_z/I_t = x \quad (59)$$

and

$$I_t = \gamma\{\pi(r_2^2 - r_1^2) \frac{RT}{F} a \exp (y_o) \quad (60)$$

In this case, there is hardly any potential variation in the pore and the current is generated uniformly in the pore. It is clear from Equation (60) that for this case, the predicted Tafel slope is the normal one of 2RT/F. When the approximation (54) cannot be made the variation of (I_z/I_t) is given by (52), according to which there would be a short linear region of slope less than 45^o followed by a curve with increasing slope. In this case, the Tafel slope is initially (i.e. at low η_o) 2RT/F, followed by a region of double the initial slope.[5]

3.3 Case of concentration and ohmic polarization

Conditions under which b exp y $>>$ 1. This condition applies when i_o and Δr are large or when D and c^o are small. Under these conditions, Equation (12) becomes

$$\frac{d^2y}{dx^2} = \frac{a \sinh y}{b \exp y}$$

$$= \frac{a}{2b}\left[1 - \exp(-2y)\right] \tag{61}$$

Using the substitution (18) and integrating the above equation

$$\left(\frac{dy}{dx}\right)^2 = \frac{a}{b}\left[(y - y_o) + \frac{1}{2}\left\{\exp(-2y) - \exp(-2y_o)\right\}\right] \tag{62}$$

It is not possible to obtain an analytic expression for the integral of (62). Analytic solutions may, however, be obtained for some limiting cases.

(i) Suppose $(y - y_o)$ is small, which corresponds to a small variation in potential in the thin film. Then, Equation (62) reduces to

$$\left(\frac{dy}{dx}\right)^2 = \frac{a}{b}(y - y_o)\left[1 - \exp(-2y_o)\right] \tag{63}$$

Integrating the above equation with boundary condition (21)

$$(y - y_o) = \frac{1}{4}\left[\frac{a}{b}\left\{1 - \exp(-2y_o)\right\}\right] x^2 \tag{64}$$

and

$$\frac{dy}{dx} = \frac{1}{2}\left[\frac{a}{b}\left\{1 - \exp(-2y_o)\right\}\right] x \tag{65}$$

Using Equation (65) in (17)

$$I_z/I_t = x \tag{66}$$

and $$I_t = \kappa\pi(r_2^2 - r_1^2)\frac{RT}{\ell F}\frac{a}{b}\left[1 - \exp(-2y_o)\right] \quad (67)$$

(ii) The second limiting case is when both y and y_o are large such that the exponential terms in y and y_o may be neglected in comparison to the corresponding linear terms. For this case,

$$(dy/dx)^2 = (a/b)(y - y_o) \quad (68)$$

and $$(y - y_o) = (a/4b) \cdot x^2 \quad (69)$$

$$dy/dx = (a/2b)\, x \quad (70)$$

For this case, too, there is a linear variation in current with distance in the thin film. This case corresponds to one of limiting current and the potential drop in the thin film is due to ohmic polarization. As compared with the previous limiting case, it may be pointed out that the former would refer to one of high exchange current density at low overpotentials and the latter one of low i_o at high overpotentials.

4. Numerical calculations and conclusions

4.1 Case where all forms of polarization are considered

As seen from Equation (21), it is possible to obtain only a numerical solution to the differential equation (12). Numerical solutions were obtained using an exchange current density of 10^{-6} amp cm^{-2} but varying (a) the product $DnFc^o$, (b) specific conductance of the electrolyte, κ, (c) the radius of the pore, r_2 and (d) the thickness

of the film, Δr. The values of these parameters used in the present calculation are shown in Table 1. Equation (21) shows that a limiting current is obtained when the overpotential reaches fairly high values and it is proportional to a/b (which proportionality is obtained after a second integration using this condition). From this condition and Equations (13) and (14), it follows that the limiting current is independent of the exchange current density. In the lower overpotential range the current density-overpotential relation is similar to that for the case of activation-ohmic polarization case (Section 3.2). It follows from Equation (12) that if the exchange current densities are smaller than 10^{-6} amp cm^{-2}, the shape of the overpotential-current density curve is similar to that shown for 10^{-6} amp cm^{-2} with the same values of $D_{nFc}{}^{o}$, r_2, Δr and γ but with a parallel shift tending towards the same limiting current densities. The current-potential relations for lower exchange current densities would show longer Tafel regions than those for higher exchange current densities. The overpotential-current density relations* are shown in Figures 2 to 4 for the various cases considered in Table 1 with $i_o = 10^{-6}$ amp cm^{-2}. The noteworthy features of these curves are:

(i) The initial shape of these curves corresponds to the case of activation-ohmic polarization considered in the next section, i.e. the role of diffusion polarization is negligible.

---

*As in a previous paper[5] the current density is taken as the product of the total current generated per pore and of the number of pores per cm^2. The number of pores cm^{-2} is $(1/4\ r_2^2)$ assuming that the parallel cylindrical pores touch each other in a cubic array.

(ii) The length of the portion corresponding to the case of activation-ohmic polarization depends on the magnitude of $DnFc^{o}$, r_2, Δr and κ in the following manner. The higher the value of $DnFc^{o}$, the longer is this region. This is also the case for the lower values of κ, Δr and r_2.

(iii) When b in Equation (14) is less than 10^{-4}, a limiting current density is not reached in the practical overpotential range (less than 0.7 v). This is more so if the exchange current density is lower than 10^{-6} amp cm^{-2}.

(iv) The limiting current density is higher, the lower is the value of Δr, the higher the value of $DnFc^{o}$, or r_2. The limiting current density is independent of the value of κ. However, for lower values of κ, the limiting current is reached at higher values of the overpotential.

(v) On comparing current density-overpotential relations for this model and the simple pore model,[5] it is readily seen that the current densities for the thin film model exceed that for the simple pore model (at the same values of the overpotential) throughout the entire range using identical kinetic parameters in both cases.

The general shapes of the current density-overpotential relations are similar in both cases. At low overpotentials, there is a short region showing the normal Tafel slope of 2RT/F which passes over into a region where the Tafel slope is 4RT/F and finally the region where the current density varies slowly with increase of overpotential close to the limiting current density of the electrode.

(vi) The current distribution plots [$(I_z/I_t$ - x (or z) relations] show a special type of behavior. In previous cases, with increase of overpotential, the current distribution tends to become more non uniform with concentration of current generation increasing at either one or the other end of the pore.[5] In the present cases, where the product $DnFc^o$ is not too high, and a limiting current is observed in the overpotential region of interest, the current generation becomes non uniform with increase of overpotential at lower overpotentials but the behavior is reversed at higher overpotentials in the regions where the current is close to the limiting current. At the limiting current, there is a uniform current distribution within the pore as is observed at low overpotentials. A typical current-distance relation is shown in Figure 5.

4.2 Case of activation and ohmic polarization

The procedure for the numerical calculations in this case are quite similar to that for the corresponding calculation of the simple pore model.[5] Thus, the calculations would be of two general types, as shown in the derivations above. For η_o values less than 0.1 V, the elliptic integral calculation is necessary. For $\eta_o >$ 0.1 V (the Tafel approximation case), the results can be expressed in a more general way.

The elliptic integral calculations have been carried out varying i_o, r_2, Δr and κ as indicated in Table 2. The only parameter which one finds in addition to the others for the simple pore model

calculation is $r_2 - r_1 = \Delta r$, the thickness of the thin film. The same values of η_o, as in the simple pore calculation, were used and are found in Table 3.

An analysis of the results of the present calculations may be best made by comparing it with the results of the similar calculation for the simple pore model[5] and may be summarized as follows:

(i) For the same value of the radius of the pore (r_2), the influence of ohmic polarization is greater for the thin film model than for the simple pore model. Thus, the current distribution becomes more non uniform at lower overpotentials for the thin film model. This effect is due to ionic conduction having to occur only through the film for the present model, whereas through the entire pore in the simple pore model. This effect is obviously less, the higher the thickness of the film.

(ii) In the present case, even with $i_o = 10^{-9}$ amp cm^{-2}, there is an effect of the ohmic-polarization at the small values of the overpotential. This was not so with the simple pore model.

At higher overpotentials, the current and potential distribution relations (Equations 49 and 50) are represented by the same figures as for the simple pore model[5] (Figures 6 and 7). These curves are given in terms of a parameter A, where A in this case is given by

$$A = \frac{a^{1/2}}{2} \exp (y_o/2)$$

$$= \frac{1}{2} \left(\frac{i_o^2 F}{\kappa(\Delta r)RT}\right)^{1/2} \exp (y_o/2) \qquad (71)$$

and I_t by

$$I_t = 8 \kappa \pi r_2 \Delta r \, (RT/\ell F) \, A \tan A \qquad (72)$$

As in the elliptic integral calculation, the current distribution becomes more non uniform at lower overpotentials for the thin film than for the simple pore model, using the same values of i_o, r_2 and χ. This trend is seen by a comparison of Table 4 for the simple pore model and Table 5 for the present model, which show the η_o values corresponding to the A values used in the calculations (and hence the different curves in Fig. 6 and 7) for various values of i_o, χ, r_2 and Δr.

The current density-overpotential relation is again similar in form to that obtained for the simple pore model and is simply obtained from the useful parameter A, except for a parallel shift both vertically and horizontally depending on the values of the kinetic parameters. A typical current density-overpotential relation is shown in Fig. 8 using $i_o = 10^{-6}$ amp cm^{-2}, $\chi = 1$ ohm^{-1} cm^{-1}, $r_2 = 10^{-4}$ cm and $r_1 = 9 \times 10^{-5}$ cm. This figure also shows the corresponding current density-overpotential relation for the simple pore model for the same value of the kinetic parameters. The current density for the simple pore model is higher than that for the thin film model at higher overpotentials.

4.3 Case of concentration and ohmic polarization

No separate calculations were carried out for this case, since the results of the first calculation carried out in the region of the limiting current are identical with those which would be obtained here. As is seen from figures 2 to 4, the current distribution becomes uniform close to the limiting current density. Further, the limiting current per pore is given by Equation (67) with $y_o \longrightarrow \infty$.

REFERENCES

1. Will, F. G., J. Electrochem. Soc., 110, 145 (1963).

2. Austin, L. G., Mariet, M., Walker, R. D., Wood, G. B. and Comyn, R. H., Ind. and Eng. Chem. (Fundamentals), 4, 321 (1965).

3. Grens, E. A., Turner, R. M. and Katan, T., Symposium on Fuel Cell Systems, Vol. 7, No. 4, 31, American Chemical Society, N. Y. (1963).

4. Bennion, D. N., Ph.D. Thesis, University of California, Berkeley (1964).

5. Srinivasan, S., Hurwitz, H. D. and Bockris, J. O'M., submitted for publication to J. Electrochem. Soc.

LIST OF TABLES

CAPTIONS TO FIGURES

1. Schematic representation of thin film model of porous electrode. Thickness of film largely exaggerated in diagram.
2. Overpotential-current density relations, for case where all forms of polarization are taken into account, showing effect of variation of γ or product $DnFc^{o}$. Kinetic parameters used in calculation are given in Table 1.
3. Overpotential-current density relations, for case where all forms of polarization are taken into account, showing effect of variation of Δr. Kinetic parameters are in Table 1.
4. Overpotential-current density relations, for case where all forms of polarization are taken into account, showing effect of variation of r_2. Kinetic parameters are in Table 1.
5. Typical current distribution relations for case where all forms of polarization are considered. Fig. 5 A and B correspond to curves 1 and 4 respectively of Fig. 2.
6. Current distribution relations for case of activation and ohmic polarization as a function of parameter A. A values are for ⊗ 0.5; ⊕ 0.6; ● 0.7; ▲ 0.8; ▼ 0.9; ○ 1.0; □ 1.1; △ 1.2; ▽ 1.3; X 1.4; + 1.45; ◐ 1.50; ◧ 1.55.
7. Potential distribution relations for case of activation and ohmic polarization as a function of parameter A. Symbols for A values are same as in Fig. 6.
8. Overpotential-current density relation for case of activation and ohmic polarization using $i_o = 10^{-6}$ amp cm^{-2}, $\gamma = 1$ ohm^{-1} cm^{-1},

$r_2 = 10^{-4}$ cm, $\Delta r = 10^{-5}$ cm, $\ell = 10^{-1}$ cm. Solid line is for thin film model. Broken line is for simple pore model (reference 5).

Table 1. Kinetic and Physical Parameters for Numerical Calculations

(Vide Figures 2-4)

Curve No. in Fig. 2-4	$DnFc^{\circ}$ amp cm^{-1}	κ ohm^{-1} cm^{-1}	r_2 cm	r cm
1	10^{-4}	1	10^{-4}	10^{-5}
2	10^{-4}	0.1	10^{-4}	10^{-5}
3	10^{-9}	1	10^{-4}	10^{-5}
4	10^{-9}	0.1	10^{-4}	10^{-5}
5	10^{-6}	1	10^{-4}	10^{-5}
6	10^{-6}	1	10^{-4}	10^{-6}
7	10^{-6}	1	10^{-3}	10^{-5}

Table 2. Kinetic and Physical Parameters for Elliptic Integral Calculations in the Case of Activation and Ohmic Polarization

i_o amp cm^{-2}	10^{-3}	10^{-6}	10^{-9}
κ ohm^{-1} cm^{-1}	0.1	1	2
r_2 cm	10^{-3}	10^{-4}	
Δr cm	10^{-4}	10^{-5}	10^{-6}

Table 3. θ Values for Elliptic Integral Calculations and Corresponding η_o Values

θ^o	η_o Volts
5	0.312
10	0.243
20	0.174
40	0.101
60	0.055
80	0.018
85	0.009

Table 4. The η_o - A Relation, Assuming K = 1 ohm^{-1} cm^{-1}, $r_2 = 10^{-4}$ cm, $\ell = 10^{-1}$ cm, for Two Values of i_o in the Case of Activation and Ohmic Polarization Using the Simple Pore Model

A	η_o volts for $i_o = 10^{-6}$ amp cm^{-2}	η_o volts for $i_o = 10^{-9}$ amp cm^{-2}
0.2	0.150	0.495
0.3	0.190	0.536
0.4	0.219	0.565
0.5	0.241	0.587
0.6	0.260	0.605
0.7	0.275	0.620
0.8	0.289	0.634
0.9	0.300	0.645
1.0	0.311	0.656
1.1	0.320	0.666
1.2	0.329	0.674
1.3	0.336	0.682
1.4	0.344	0.690
1.45	0.348	0.693
1.50	0.351	0.697
1.55	0.354	0.700

Table 5. The η_o - A Relation, Assuming κ = 1 ohm^{-1} cm^{-1}, $\Delta r = 10^{-5}$ cm, $\ell = 10^{-1}$ cm for Two Values of i_o in the Case of Activation and Ohmic Polarization Using the Thin Film Model

A	η_o volts for $i_o = 10^{-6}$ amp cm^{-2}	η_o volts for $i_o = 10^{-9}$ amp cm^{-2}
0.2	0.069	0.415
0.3	0.110	0.456
0.4	0.139	0.485
0.5	0.161	0.507
0.6	0.179	0.525
0.7	0.195	0.541
0.8	0.208	0.554
0.9	0.220	0.566
1.0	0.230	0.576
1.1	0.240	0.586
1.2	0.248	0.594
1.3	0.256	0.602
1.4	0.264	0.610
1.45	0.267	0.613
1.50	0.271	0.617
1.55	0.274	0.620

Thin Film Model

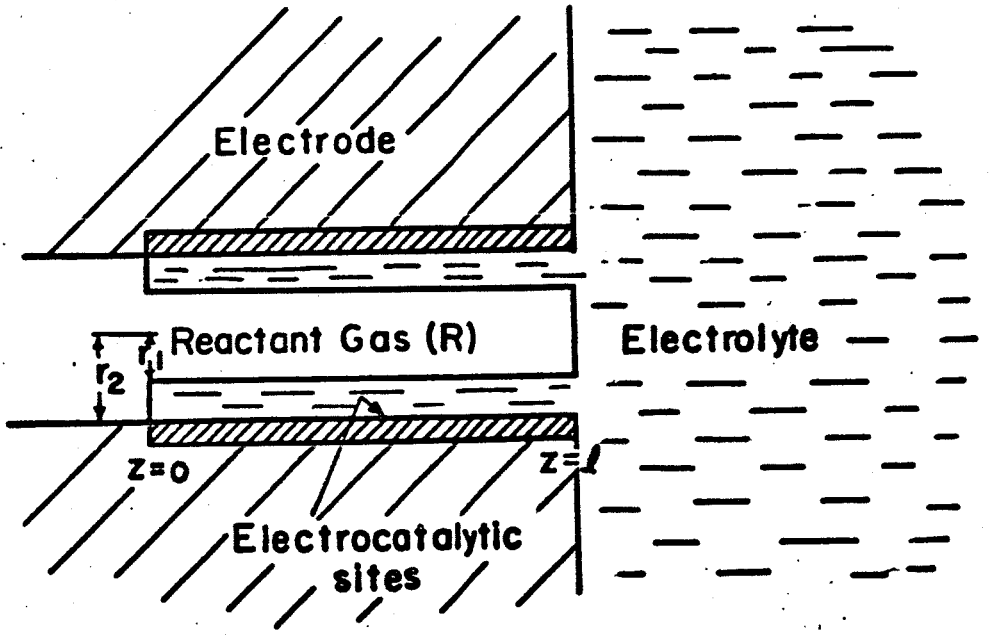

FIG.1

APX

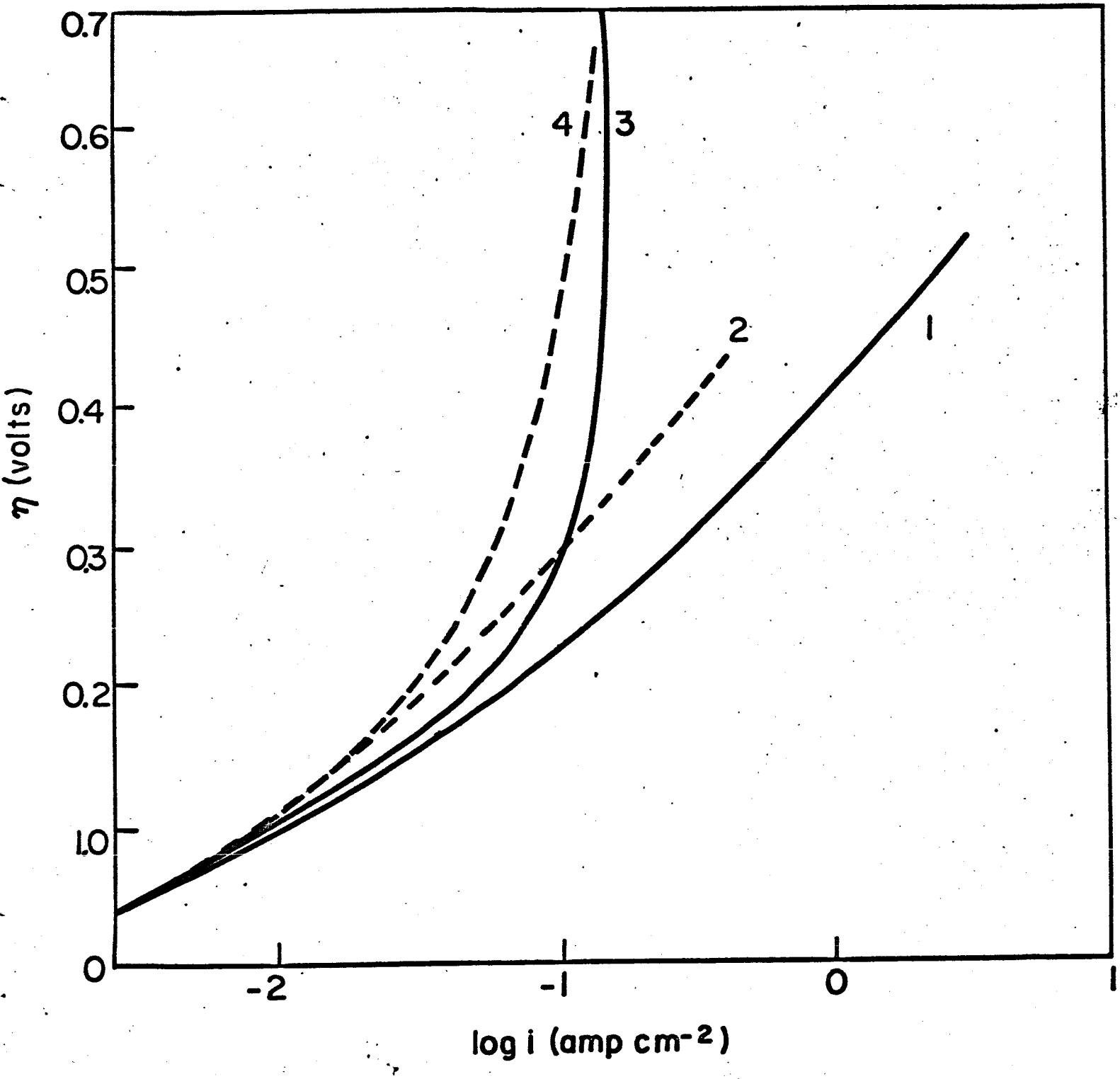

FIG. 2

APX

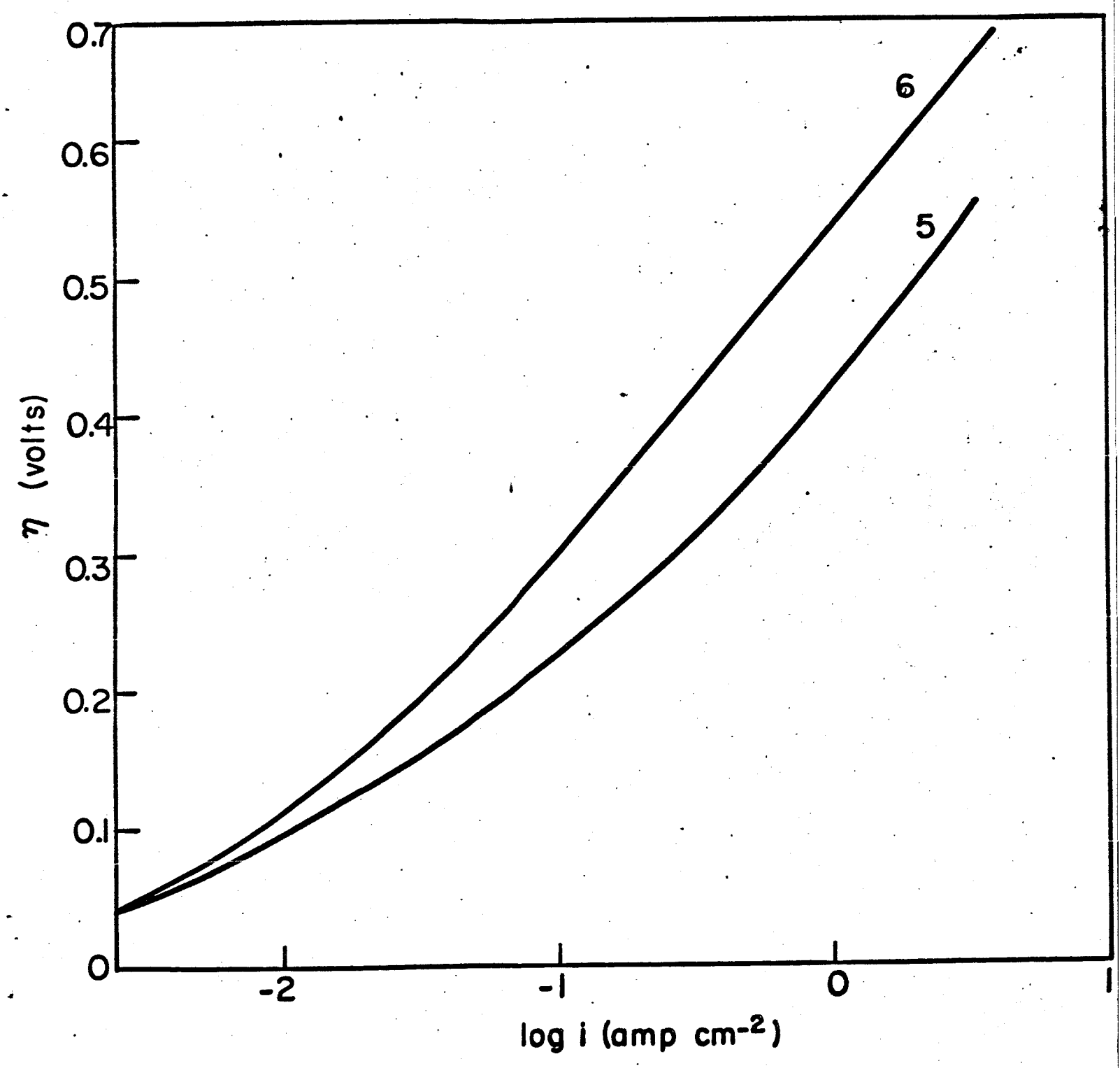

FIG. 3

APR

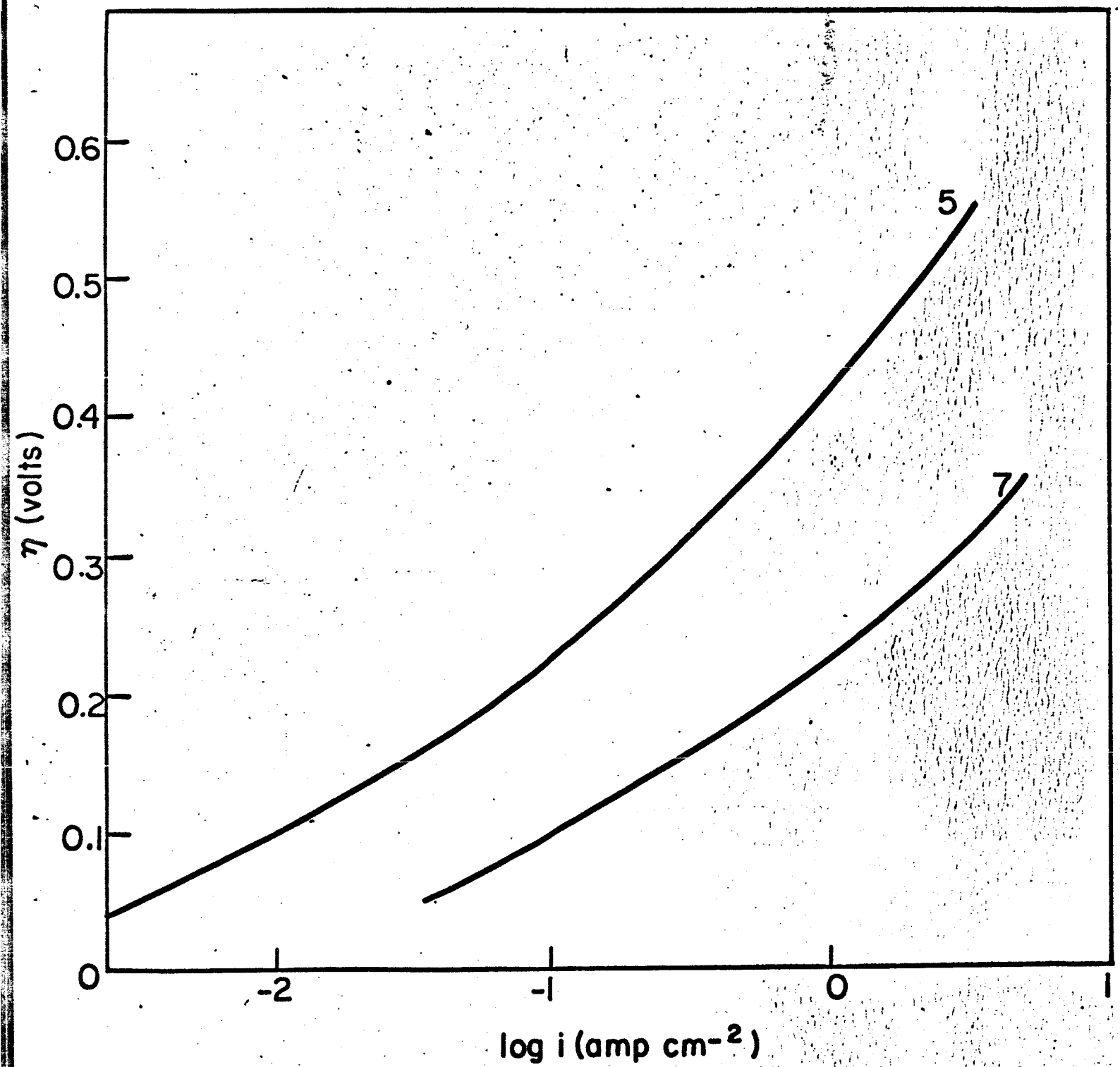

FIG.4

APX

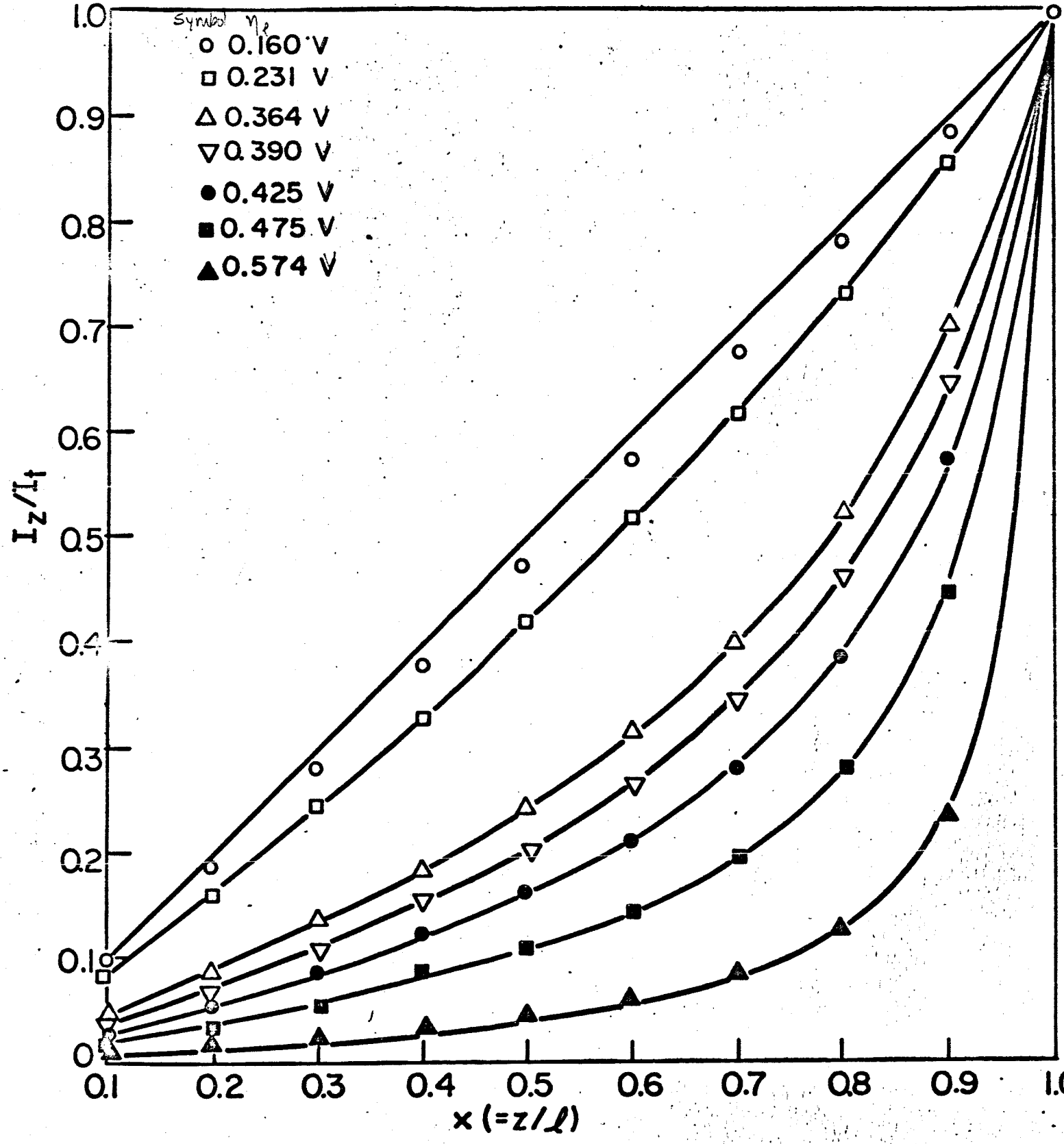
Symbol η_e
o 0.160 V
□ 0.231 V
△ 0.364 V
▽ 0.390 V
● 0.425 V
■ 0.475 V
▲ 0.574 V
I_z/I_t
x (=z/ℓ)
0
0.1
0.2
0.3
0.4
0.5
0.6
0.7
0.8
0.9
1.0

FIG. 5a

APX

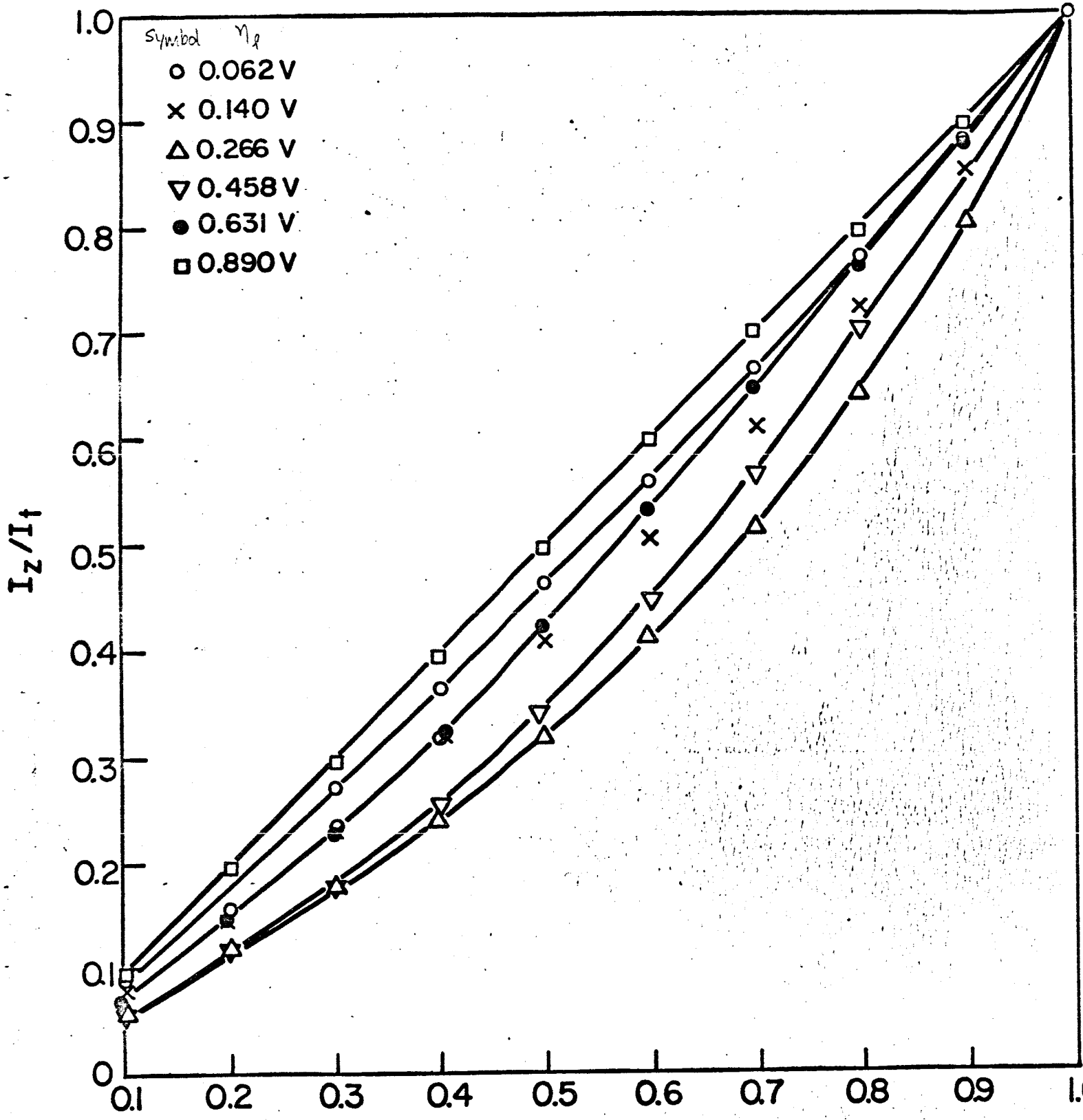
Symbol η_ℓ
o 0.062 V
× 0.140 V
△ 0.266 V
▽ 0.458 V
● 0.631 V
□ 0.890 V
I_z/I_t
$x(=z/\ell)$
0
0.1
0.2
0.3
0.4
0.5
0.6
0.7
0.8
0.9
1.0

FIG. 5b

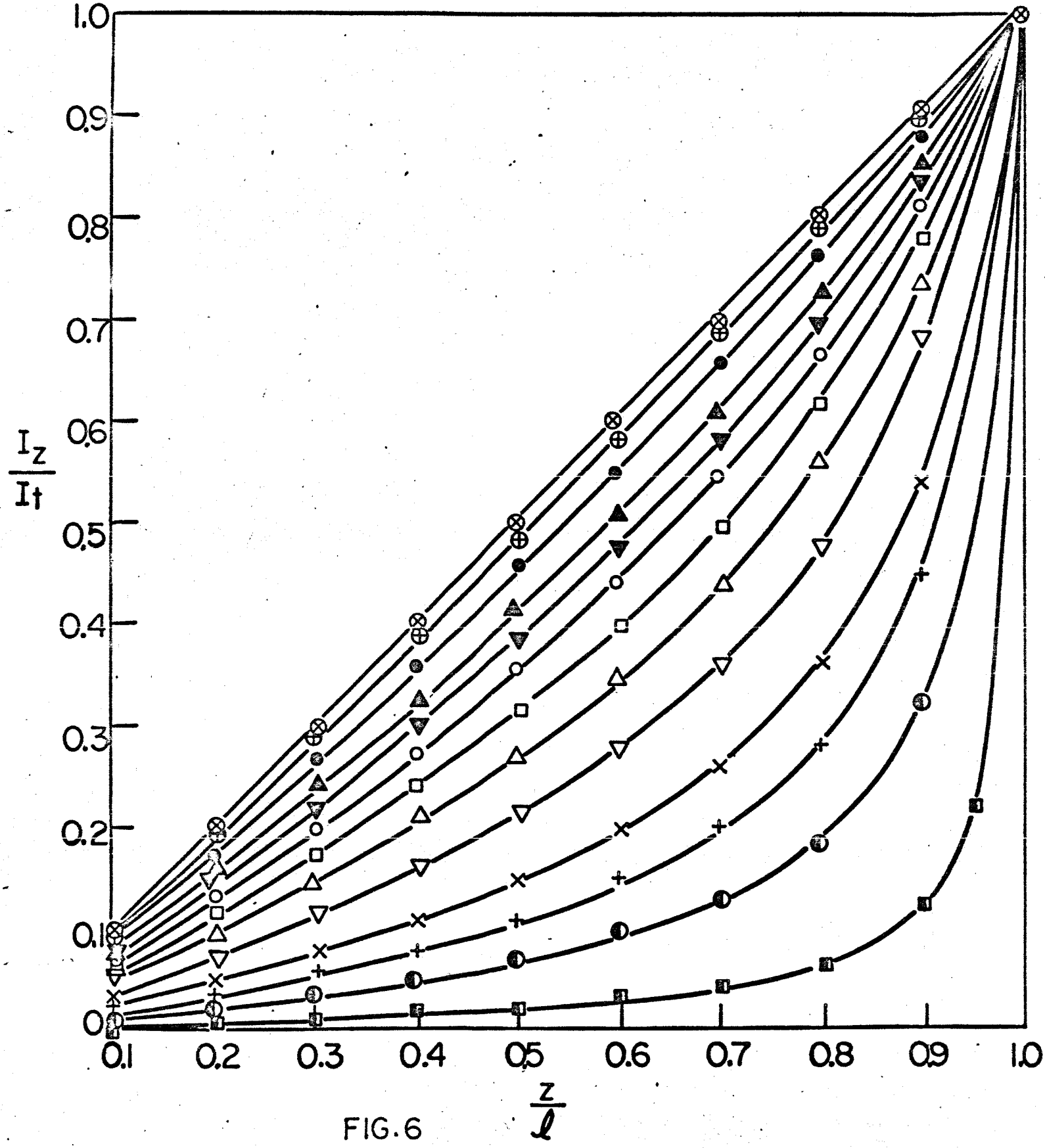
1.0
0.9
0.8
0.7
0.6
0.5
0.4
0.3
0.2
0.1
0
$\frac{I_z}{I_t}$
0.1
0.2
0.3
0.4
0.5
0.6
0.7
0.8
0.9
1.0
$\frac{z}{\ell}$

FIG. 6

APX

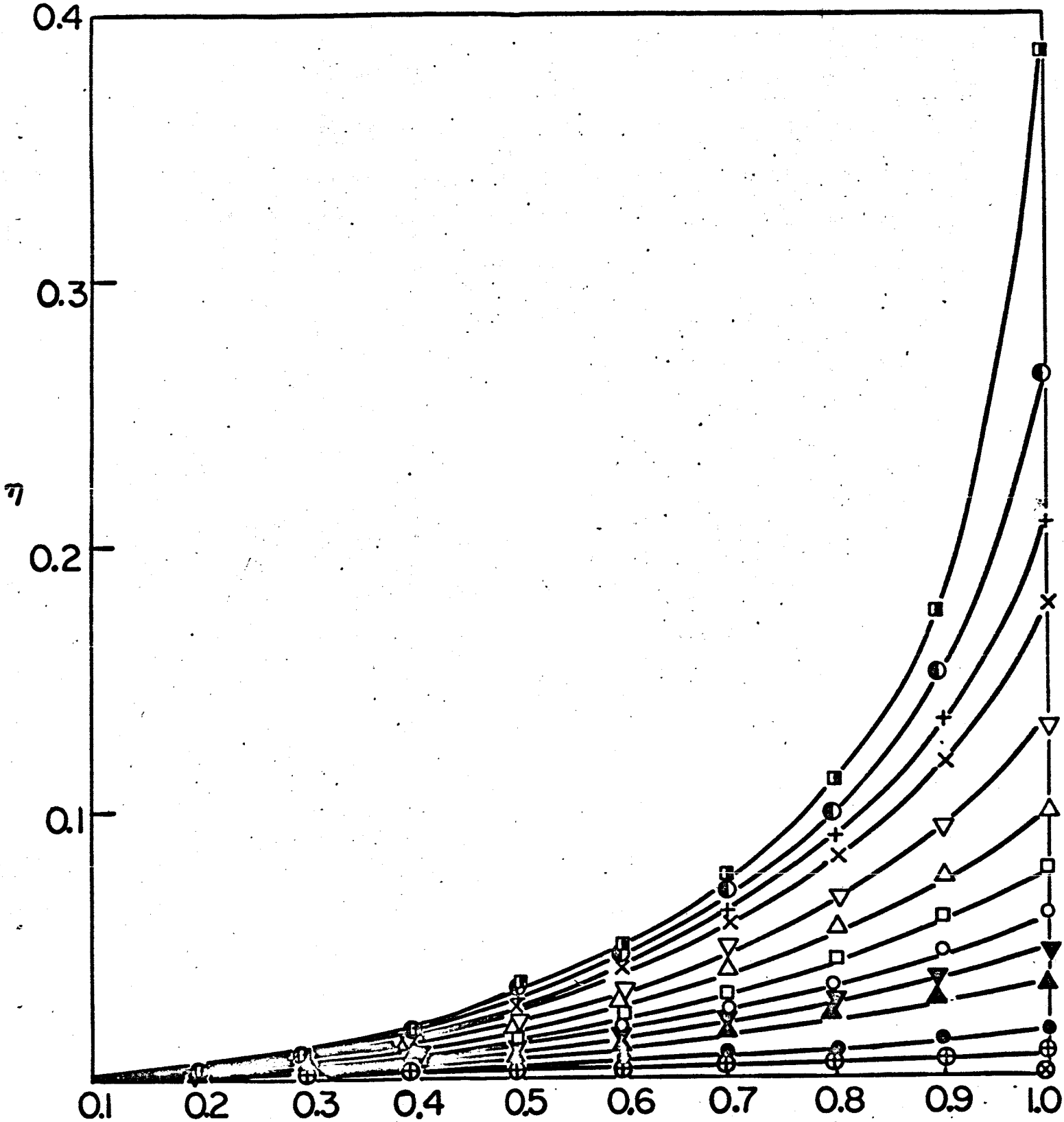

FIG. 7

APK

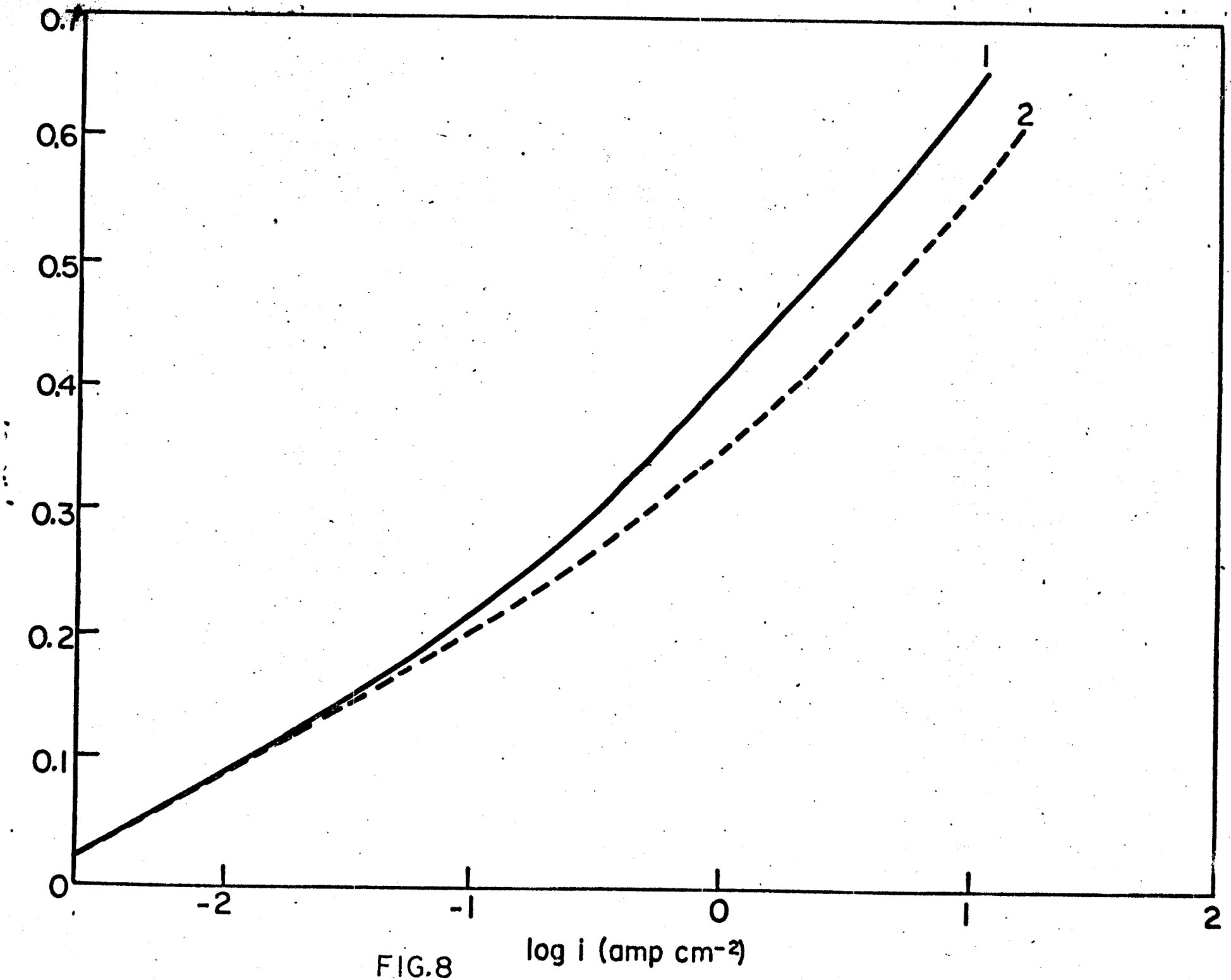

FIG.8

VIII DISTRIBUTION LIST FOR FUEL CELL REPORTS

National Aeronautics & Space Administration
Washington, D. C. 20546
Attn: Ernst M. Cohn, Code RNW
George F. Esenwein, Code MAT
A. M. Andrus, Code ST
J. R. Miles, Code SL

National Aeronautics & Space Administration
Scientific and Technical Information Facility
P. O. Box 5700
Bethesda, Maryland, 20014 (3)

National Aeronautics & Space Administration
Goddard Space Flight Center
Greenbelt, Maryland
Attn: Thomas Hennigan

National Aeronautics & Space Administration
Langley Research Center
Langley Station
Hampton, Virginia
Attn: S. T. Peterson

National Aeronautics & Space Administration
Lewis Research Center
21000 Brookpark Road
Cleveland 35, Ohio
Attn: N. D. Sanders
Robert Miller
Robert L. Cummings

National Aeronautics & Space Administration
Marshall Space Flight Center
Huntsville, Alabama
Attn: Philip Youngblood

National Aeronautics & Space Administration
Ames Research Center
Pioneer Project
Moffett Field, California
Attn: James R. Swain

Cell Reports (con't)

National Aeronautics & Space Administration
Manned Spacecraft Center
Houston 1, Texas
Attn: Richard Ferguson (for EP-5)
Robert Cohen
Forrest E. Eastman, EE-4

National Aeronautics & Space Administration
Ames Research Center
Mountain View, California
Attn: Jon Rubenzer, Biosatellite Project

Jet Propulsion Laboratory
4800 Oak Grove Drive
Pasadena, California
Attn: Aiji Uchiyama

DEPARTMENT OF THE ARMY

U.S. Army Engineer R & D Labs.
Fort Belvoir, Virginia
Attn: Electrical Power Branch

U. S. Army Engineer R & D Labs.
Fort Monmouth, New Jersey
Attn: Arthur F. Daniel (Code SELRA/SL-PS)

U. S. Army R & D Liaison Group (9851 DV)
APO 757
New York, New York
Attn: Chief, Chemistry Branch

U. S. Army Research Office
Physical Sciences Division
3045 Columbia Pike
Arlington, Virginia

Harry Diamond Labs.
Room 300, Building 92
Connecticut Avenue & Van Ness Street, N. W.
Washington, D. C.
Attn: Nathan Kaplan

Cell Reports (con't.)

Army Material Command
Research Division
AMCRD-RSCM T-7
Washington 25, D.C.
Attn: John W. Crellin

Natick Labs.
Clothing & Organic Materials Div.
Natick, Massachusetts
Attn: Leo A. Spano/Robert N. Walsh

U. S. Army TRECOM
Physical Sciences Group
Fort Eustis, Virginia
Attn: (SMOFE)

U. S. Army Research Office
Box CM, Duke Station
Durham, North Carolina
Attn: Paul Greer/Dr. Wilhelm Jorgensen

U. S. Army Mobility Command
Research Division
Center Line, Michigan
Attn: O. Renius (AMSMO-RR)

Hq., U. S. Army Material Command
Development Division
Washington 25, D.C.
Attn: Marshall D. Aiken (AMCRD-DE-MO-P)

DEPARTMENT OF THE NAVY

Office of Naval Research
Department of the Navy
Washington 25, D. C.
Attn: Dr. Ralph Roberts/H.W. Fox

Cell Reports (con't.)

Mr. J. H. Harrison
Special Projects Division
U. S. Navy Marine Engineering Lab.
Annapolis, Maryland 21402

Bureau of Naval Weapons
Department of the Navy
Washington 25, D.C.
Attn: (Code RAAE)

U. S. Naval Research Laboratory
Washington, D.C., 20390
Attn: (Code 6160)

Bureau of Ships
Department of the Navy
Washington 25, D.C.
Attn: Bernard B. Rosenbaum/C. F. Viglotti

Naval Ordnance Laboratory
Department of the Navy
Corona, California
Attn: Mr. William C. Spindler (Code 441)

Naval Ordnance Laboratory
Department of the Navy
Silver Spring, Maryland
Attn: Philip B. Cole (Code WB)

DEPARTMENT OF THE AIR FORCE

Wright-Patterson AFB
Aeronautical Systems Division
Dayton, Ohio
Attn: George W. Sherman, APIP

AF Cambridge Research Lab
Attn: CRZE
L. G. Hanscom Field
Bedford, Massachusetts
Attn: Francis X. Doherty/Edward Rasking (Wing F)

Cell Reports (cont'd)

Rome Air Development Center, ESD
Griffiss AFB, New York
Attn: Frank J. Mollura (RASSM)

Space Systems Division
Attn: SSZAE-11
Air Force Unit Post Office
Los Angeles 45, California

Air Force Ballistic Missile Division
Attn: WEZYA-21
Air Force Unit Post Office
Los Angeles 45, California

ATOMIC ENERGY COMMISSION

Mr. Donald B. Hoatson
Army Reactors, DRD
U. S. Atomic Energy Commission
Washington 25, D. C.

OTHER GOVERNMENT AGENCIES

Office, DDR&E: USW & BSS
The Pentagon
Washington 25, D. C.
Attn: G. B. Wareham

Mr. Kenneth B. Higbie
Staff Metallurgist
Office, Director of Metallurgy Research
Bureau of Mines
Interiof Building
Washington, D. C., 20240

Institute for Defense Analyses
Research & Engineering Support Division
400 Army-Navy Drive
Arlington, Virginia 22202
Attn: Dr. George C. Szego/R. Hamilton

Cell Reports (cont'd)

Power Information Center
University of Pennsylvania
Moore School Building
200 South 33rd Street
Philadelphia 4, Pennsylvania

Chief, Input Section, CFSTI
Sills Building
5285 Port Royal Road
Springfield, Virginia, 22151

PRIVATE INDUSTRY

Alfred University
Alfred, New York
Attn: Professor T. J. Gray

Allis-Chalmers Mfg. Co.
1100 S. 70th Street
Milwaukee 1, Wisconsin
Attn: Dr. W. Mitchell, Jr.

Allison Division of General Motors
Indianapolis 6, Indiana
Attn: Dr. Robert E. Henderson

American Cyanamid Company
1937 W. Main Street
Stamford, Connecticut
Attn: Dr. R. G. Haldeman

American Machine & Foundry
689 Hope Street
Springdale, Connecticut
Attn: Dr. L. H. Shaffer
Research & Development Division

Cell Reports (cont'd.)

Astropower, Inc.
2968 Randolph Avenue
Costa Mesa, California
Attn: Dr. Carl Berger

Battelle Memorial Institute
Columbus 1, Ohio
Attn: Dr. C. L. Faust

Bell Telephone Laboratories, Inc.
Murray Hill, New Jersey
Attn: Mr. U. B. Thomas

Clevite Corporation
Mechanical Research Division
540 East 105 th Street
Cleveland, Ohio
Attn: A. D. Schwope

Electrochimica Corp.
1140 O'Brien Drive
Menlo Park, California
Attn: Dr. Morris Eisenberg

Electro-Optical Systems, Inc.
300 North Halstead Street
Pasadena, California
Attn: E. Findl

Engelhard Industries, Inc.
497 DeLancy Street
Newark 5, New Jersey
Attn: Dr. J. G. Cohn

Esso Research & Engineering Company
Products Research Division
P. O. Box 215
Linden, New Jersey
Attn: Dr. Carl Heath

Cell Reports (con'd.)

The Franklin Institute
Philadelphia, Pennsylvania
Attn: Mr. Robert Goodman

General Electric Company
Direct Energy Conversion Operations
Lynn, Massachusetts
Attn: Dr. E. Glazier

Garrett Corp.
1625 Eye St., N. W.
Washington 6, D. C.
Attn: George R. Shepherd

General Electric Company
Research Laboratory
Schenectady, New York
Attn: Dr. H. Liebhafsky

General Electric Company
Missile and Space Division (Room M133S)
P. O. Box 8555
Philadelphia 1, Pennsylvania
Attn: L. Chasen

General Motors Corp.
Box T
Santa Barbara, California
Attn: Dr. C. R. Russell

Globe-Union, Inc.
Milwaukee 1, Wisconsin
Attn: Dr. C. K. Morehouse

Dr. Joseph S. Smatko
General Motors
Defense Research Laboratories
P. O. Box T
Santa Barbara, California, 93102

Cell Reports (cont'd.)

John Hopkins University
Applied Physics Laboratory
8621 Georgia Avenue
Silver Springs, Maryland
Attn: W. A. Tynan

Leesona Moos Laboratories
Lake Success Park
Community Drive
Great Neck, New York
Attn: Dr. A. Moos

McDonnell Aircraft Corporation
Attn: Project Gemini Office
P. O. Box 516
St. Louis 66, Missouri

Monsanto Research Corporation
Everette 49, Massachusetts
Attn: Dr. J. O. Smith

North American Aviation Co.
S & ID Division
Downey, California
Attn: Dr. James Nash

Pratt and Whitney Aircraft Division
United Aircraft Corporation
East Hartford 8, Connecticut
Attn: Librarian

Radio Corporation of America
Astro Division
Heightstown, New Jersey
Dr. Seymour Winkler

Radio Corporation of America
Somerville, New Jersey
Attn: Dr. G. Lozier

Cell Reports (cont'd.)

Speer Carbon Company
Research And Development Laboratories
Packard Road at 47th Street
Niagara Falls, New York
Attn: Dr. L. M. Liggett

Stanford Research Institute
820 Mission Street
So. Pasadena, California
Attn: Dr. Fritz Kalhammer

Thiokol Chemical Corporation
Reaction Motors Division
Denville, New Jersey
Attn: Dr. D. J. Mann

Thompson Ramo Wooldridge
2355 Euclid Avenue
Cleveland 17, Ohio
Attn: Mr. Vittor Kovacik

Unified Science Associates, Inc.
826 S. Arroyo Parkway
Pasadena, California
Attn: Dr. Sam Naiditch

Union Carbide Corporation
12900 Snow Road
Parma, Ohio
Attn: Dr. George E. Evans

University of California
Space Science Laboratory
Berkeley 4, California
Attn: Prof. Charles W. Tobias

University of Pennsylvania
Philadelphia 4, Pennsylvania
Attn: Dr. Manfred Altman

Cell Reports (cont'd.)

Western Reserve University
Cleveland, Ohio
Attn: Prof. Ernest Yeager

Yardney Electric Corp.
New York, New York
Attn: Dr. Paul Howard

Lockheed Missiles & Space Co.
3251 Hanover St.
Palo Alto, California
Attn: Dr. George B. Adams

Mr. B. S. Baker
Institute of Gas Technology
State & 34th Streets
Chicago 16, Illinois

Mr. Peter D. Richman
President
Chem Cell Inc.
3 Central Ave.
East Newark, New Jersey 07029